A FLOW VELOCITY AND DIRECTION INSTRUMENT

A Thesis

Presented to

the Faculty of the School of Engineering and Applied Science

University of Virginia

In Partial Fulfillment

of the Requirements for the Degree

Master of Science in Electrical Engineering

by

James H. Monteith

August 1970

APPROVAL SHEET

This thesis is submitted in partial fulfillment of

the requirements for the degree of

Master of Science in Electrical Engineering

_____

Author

Approved:

_____

Faculty Adviser

_____

Dean, School of Engineering
and Applied Science

August 1970

ACKNOWLEDGMENTS

Acknowledgment is given to Mr. Donald L. Maiden of the National Aeronautics and Space Administration, Langley Research Center for the design of the positioning technique used in this instrument. The author wishes to extend his gratitude to Langley Research Center for supporting this thesis. Appreciation is also expressed to Dr. E. S. McVey of the University of Virginia for his valuable guidance and helpful criticisms.

TABLE OF CONTENTS

LIST OF TABLES

LIST OF FIGURES

LIST OF SYMBOLS

$\overline{A}$	vector used to relate $\hat{\rho}_1$, $\hat{\rho}_2$, and $\hat{v}$ to the x,y,z coordinate reference, in.
$\hat{a}$	unit vector of $\overline{A}$
$\overline{B}$	same as $\overline{A}$, in.
$\hat{b}$	unit vector of $\overline{B}$
b_o	stall torque of servomotor for a given input voltage, oz-in.
$\overline{C}$	same as $\overline{A}$, in.
$\hat{c}$	unit vector of $\overline{C}$
$\overline{D}$	same as $\overline{A}$, in.
$\hat{d}$	unit vector of $\overline{D}$
e_a	motor input voltage, V
e_g	generator feedback voltage, V
e_t	output voltage of pressure transducer signal conditioner, V
e_ϵ	error voltage of inner servo loop, V
G'(S)	transfer function of amplifier-motor-generator servo loop
G(S)	transfer function of generalized control system with disturbances moved outside the loop
h	ratio of servomotor torque to speed, oz-in-sec-rad^{-1}
$\hat{i},\hat{j},\hat{k}$ $\hat{i}',\hat{j}',\hat{k}'$	unit vectors along coordinate axes of orthogonal reference systems (x,y,z) and (x',y',z')
j	imaginary quantity
J	system inertia, oz-in-sec^2-rad^{-1}
k	ratio of servomotor stall torque to input voltage, oz-in-V^{-1}

k_a	servoamplifier gain
k_g	ratio of generator feedback voltage to shaft velocity, V-sec-rad^{-1}
k_n	gear ratio of control angle (θ) to motor shaft angle (θ_m)
k_p	ratio of the pressure difference between ports to the angular deviation of the port and velocity vectors from 90°, psi-rad^{-1}
k_t	ratio of the output voltage of the pressure transducer signal conditioner to the pressure being sensed by the transducer, V-psi^{-1}
K_T	system gain, sec^{-2}
k_v	sensitivity factor relating angular deviation of port and velocity vectors from 90° to control angle changes $\left(\frac{\partial \phi}{\partial \theta}\right)$
K_V	system velocity-error constant, sec^{-1}
L	torque delivered by the servomotor, oz-in
m	sin 22.5° = 0.384
n	cos 22.5° = 0.924
psid	pressure in pounds per square inch, differential
psf	pressure in pounds per square foot
P	pressure difference between ports, psi
R	reference input to servosystem, rad
q	dynamic pressure, psi
S	Laplace-transform operator
t	time variable, sec
$\hat{v}$	velocity unit vector

x_p	distance from (x,y,z) origin to the probe tip along the X-axis, in.
α	pitch angle of probe (pitch up = +, by definition), rad
γ	inverse of time constant due to pressure tubing lag, sec^{-1}
θ	angular motion used to position probe (control angle), rad
θ'	positioning angle for null condition, rad
θ_ϵ	angular deviation of θ from its null position (i.e., $\theta_\epsilon = \theta' - \theta$), rad
θ_m	motor shaft angular position, rad
$\hat{\rho}$	unit vector describing the orientation of the pressure ports
τ	system equivalent time constant, sec
ϕ	angular deviation of the port and velocity vectors from 90°, rad
ϕ_ϵ	portion of ϕ due to the difference of the control angle from its null position (i.e., due to θ_ϵ), rad
ϕ_d	portion of ϕ due to a disturbance caused by motion of the other system's control angle, rad
ψ	yaw angle of probe (yaw right = +, by definition), rad
ω_m	angular velocity of servomotor shaft, $rad\text{-}sec^{-1}$
$(\ )_1$	subscript 1 refers to all functions in the servosystem controlling θ_1
$(\ )_2$	subscript 2 refers to all functions in the servosystem controlling θ_2

ABSTRACT

Analyses and experimental results are presented on a control system used for positioning a null seeking pressure probe. The probe is to be used in wind tunnels to measure wind velocity magnitude and direction. Two, interacting, positioning servomechanisms were used to control the pressure probe. The analysis of this system was accomplished using vector analysis as well as standard servoanalysis methods. These analyses showed the stability of the system to be dependent on the orientation of the null sensing pressure ports on the probe face. Laboratory and wind tunnel tests showed that the probe yaw and pitch angle measurements were accurate to within $\pm 1^{\circ}$ for angles up to 45°. The development of this probe has resulted in a new useful instrument for wind tunnel research.

CHAPTER I

INTRODUCTION

In wind tunnel research it has become more and more necessary to study the three-dimensional flow characteristics around the model. The magnitude and angular orientation of the airflow are of particular interest to the researchers. Various techniques and probe types have been designed to obtain this information (refs. 1-5). In small tunnels fixed probes are often used. Calibrated relations of the pressures between ports situated at various places on the face of the probe yield the desired flow characteristics (refs. 6-10). In larger tunnels or on aircraft automatic null-seeking probes can be used (ref. 11). This type of probe seeks out the direction of the wind velocity vector, and then by standard pitot techniques determines its magnitude. One of these probes has been developed at the National Aeronautics and Space Administration's Langley Research Center.

It is necessary that measuring apparatus interrogating a point in space disturb the flow characteristics as little as possible. This specification along with those that follow presented a formidable problem in the design of the probe. The other specifications are:

1. The probe shall be capable of nulling on yaw and pitch angles up to $\pm 45^{\circ}$.

2. These angles shall be determined accurately to within $\pm 1^{\circ}$.

3. Flow velocity magnitude shall be determined accurately to within ± 1 per cent over a range of velocities corresponding to dynamic pressure between 2 and 200 psf.

4. The probe tip shall maintain a given point in space while searching for a null.

This last specification made it necessary to design a unique positioning apparatus. A mechanism employing two angular motions which were not directly related to the yaw and pitch angles was designed to drive the probe to a given yaw and pitch configuration. The control of the mechanism involves two, interacting, positioning servos, since one of the motions is superimposed on the other. Most conventional positioning servos are one-dimensional in nature, requiring just one linear or angular motion. The control problem for this probe is a little more complex because of the positioning interaction. Three-dimensional vector analysis techniques are needed to analyze the feedback control systems used.

The purpose of this paper is to describe the techniques used in synthesizing the control systems. The mathematical analysis of the systems is also developed. Before discussing the control systems a description is given of the probe and the method used for positioning it. This includes an analysis of how yaw and pitch angles are related to the angles of the controlling motions. The block diagrams and the system equations are then developed. This is followed by the experimental results of wind tunnel and laboratory tests. A discussion of stability and error criteria is included. The paper concludes with a recommendation for future work and a commentary on the probe's limitations and advantages.

CHAPTER II

PROBE DESCRIPTION

To understand the analysis of the control systems one must first understand the method for positioning the probe. There are five pressure ports on the hemispherical face of the pitot-type probe (refer to Figure 1). The axial port (5) is connected to one side of a differential pressure transducer, and the static ports on the body of the probe are connected to the other side of the transducer. This differential pressure is used to yield flow velocity data after the probe has found a null and is aligned with the velocity vector. The other four ports consist of two sets of diagonal pairs (1-2 and 3-4). Each pair is connected to a differential pressure transducer which provides error signals for one of the two positioning servomechanisms controlling θ_1 and θ_2. When the probe is in a nulled condition the pressures on the ports are equal, and thus, the error signals are zero. In this condition axis 3 is colinear with the velocity vector. The axis of the pitot-type probe (axis 3) is the generatrix of a $22\text{-}1/2^{\circ}$ conical surface when revolved (θ_2) about axis 2. Axis 2 is likewise, the generatrix of a second $22\text{-}1/2^{\circ}$ conical surface when revolved (θ_1) about axis 1. This is the axis to which yaw and pitch angles are referenced. If the condition is met that the vertex angles of the two cones are equal, then rotations θ_1 and θ_2 allow the probe to assume any orientation within the confines of a third cone. This cone has a

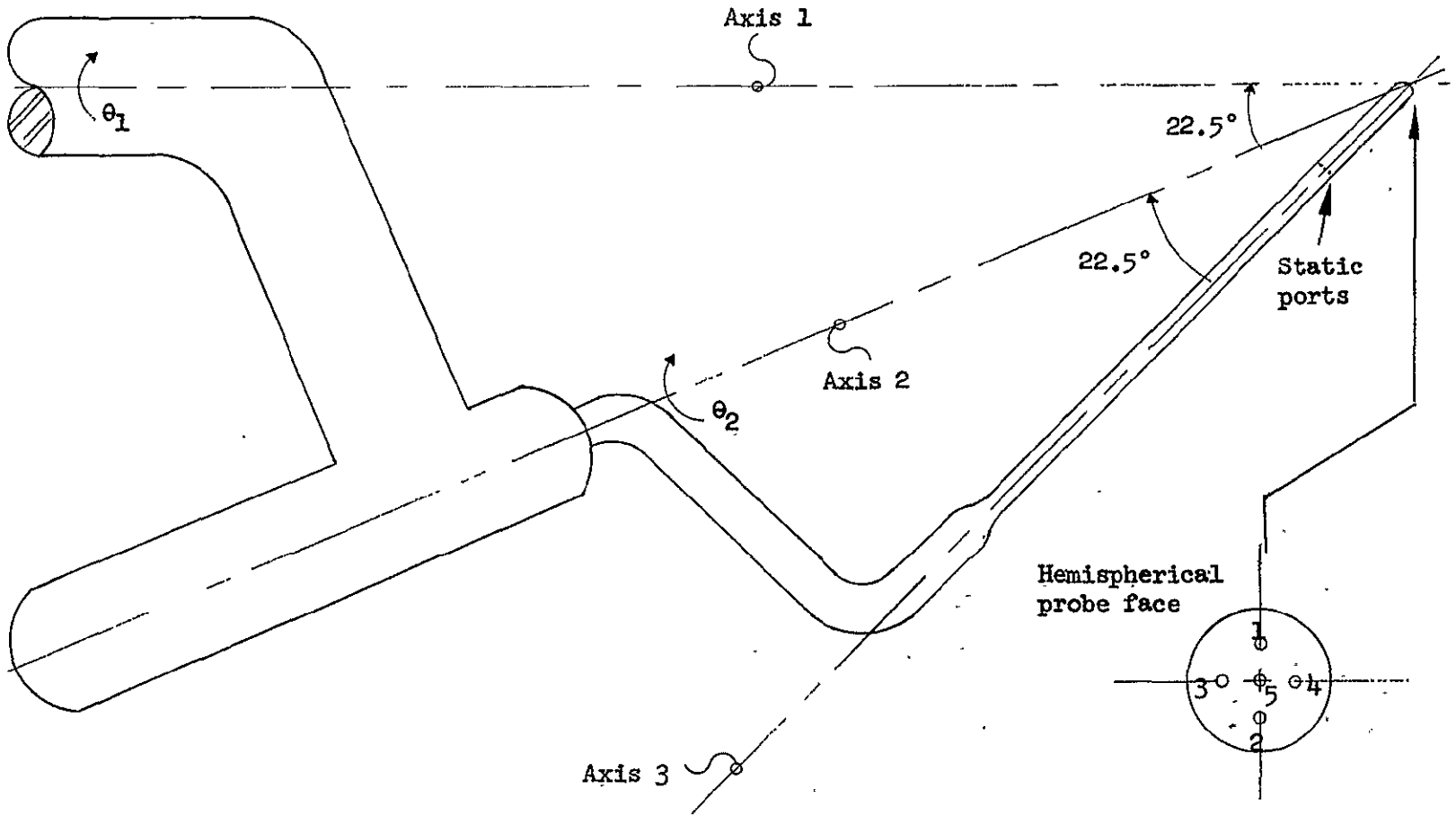

Figure 1. Flow velocity and direction probe.

45° vertex angle. Thus, the probe can assume yaw and pitch angles up $\pm 45^{\circ}$, while the probe tip maintains a given point in space.

Pressure lines run from the ports to the transducers located in the main body of the probe (axis 1). Flexible tubing is used to link the fixed lines of the pressure ports to the transducer inputs (see Figure 2). Because of these pressure lines, the motion of θ_2 must be limited to $\pm 180^{\circ}$. It is also necessary to limit the motion of θ_1 to $\pm 180^{\circ}$ due to electrical lines running to the motor, generator and synchro used to control and sense the position of θ_2.

Yaw and pitch angle determinations.- Figures 3 and 4 illustrate the orthogonal coordinate systems which are used to relate the control motions to the probe's yaw and pitch orientation (ref. 12). The $\hat{i} - \hat{j} - \hat{k}$ coordinate system is fixed on the support axis of the probe (axis 1). The $\hat{i}' - \hat{j}' - \hat{k}'$ coordinate system is located a fixed distance from the $\hat{i} - \hat{j} - \hat{k}$ origin as is shown by the vector $\overline{A}$. The orientation of the supporting member between axis 1 and axis 2 is represented by $\hat{k}'$. Axis 3, the axis of the sensing probe, is colinear with $\overline{C}$. The location of the tail of vector $\overline{C}$ with respect to the $\hat{i}' - \hat{j}' - \hat{k}'$ origin is identified by $\overline{B}$. Axis 2 is, likewise, represented by $\overline{D}$ and is colinear with $\hat{i}'$. The probe tip is situated a fixed distance x_p from the origin of the $\hat{i} - \hat{j} - \hat{k}$ system. With the probe in the positions shown in Figure 3, θ_1 and θ_2 are arbitrarily chosen to be 0°. Clockwise motions of θ_1 and θ_2 have been chosen as positive, or increasing angles. Yaw and pitch

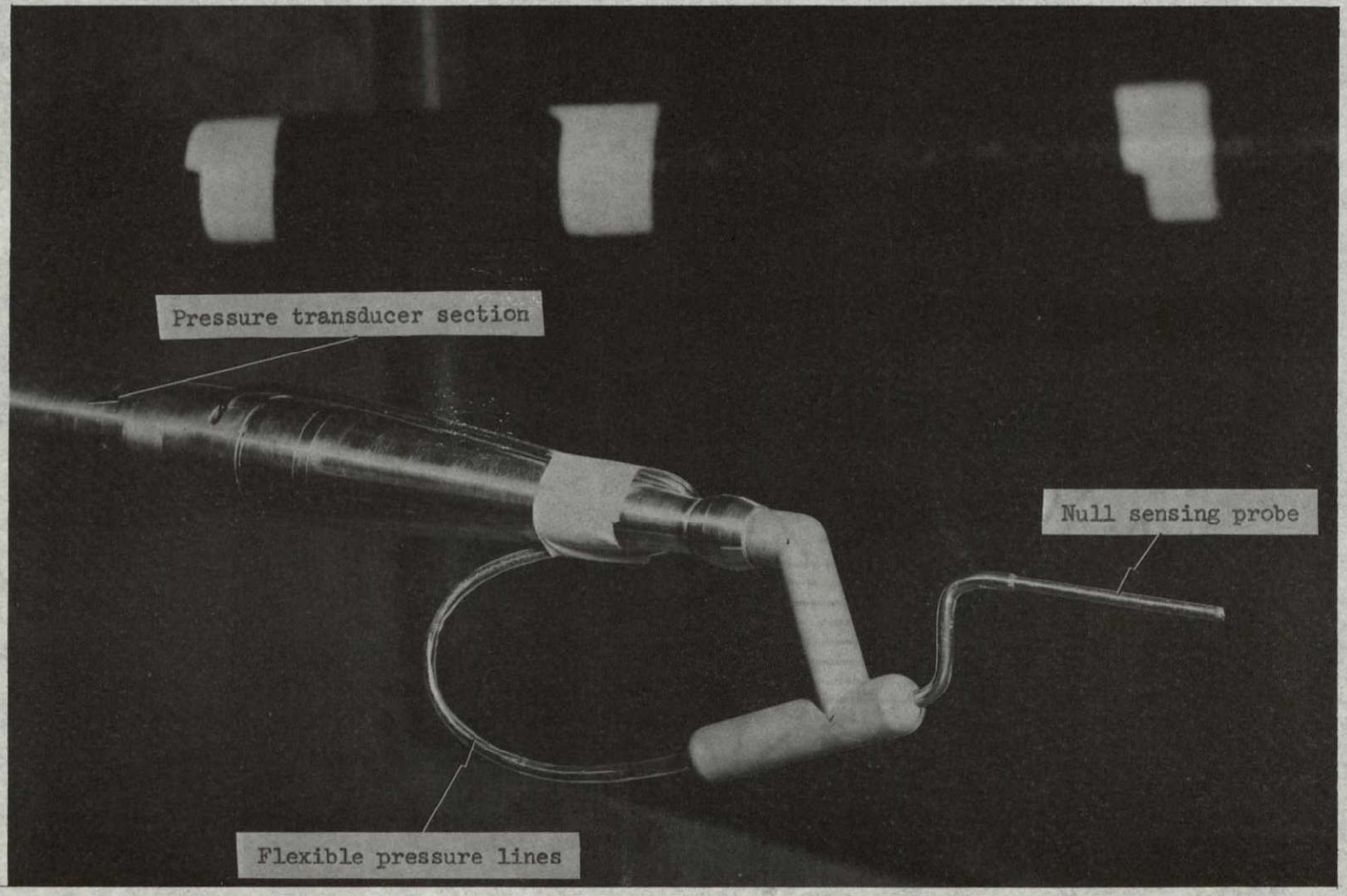

Figure 2. Probe mounted in tunnel sting.

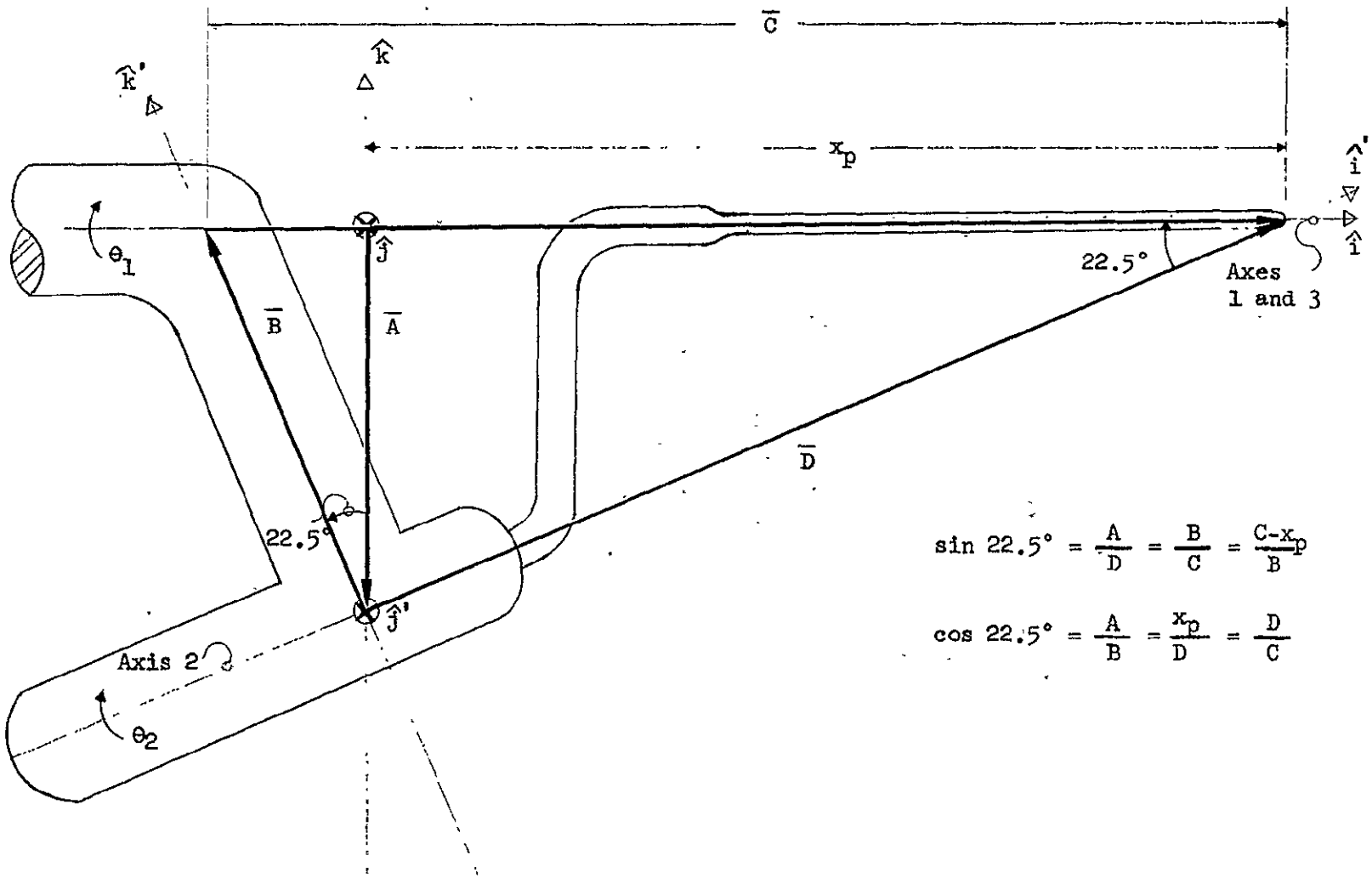

Figure 3. Vector relationship of probe parts.

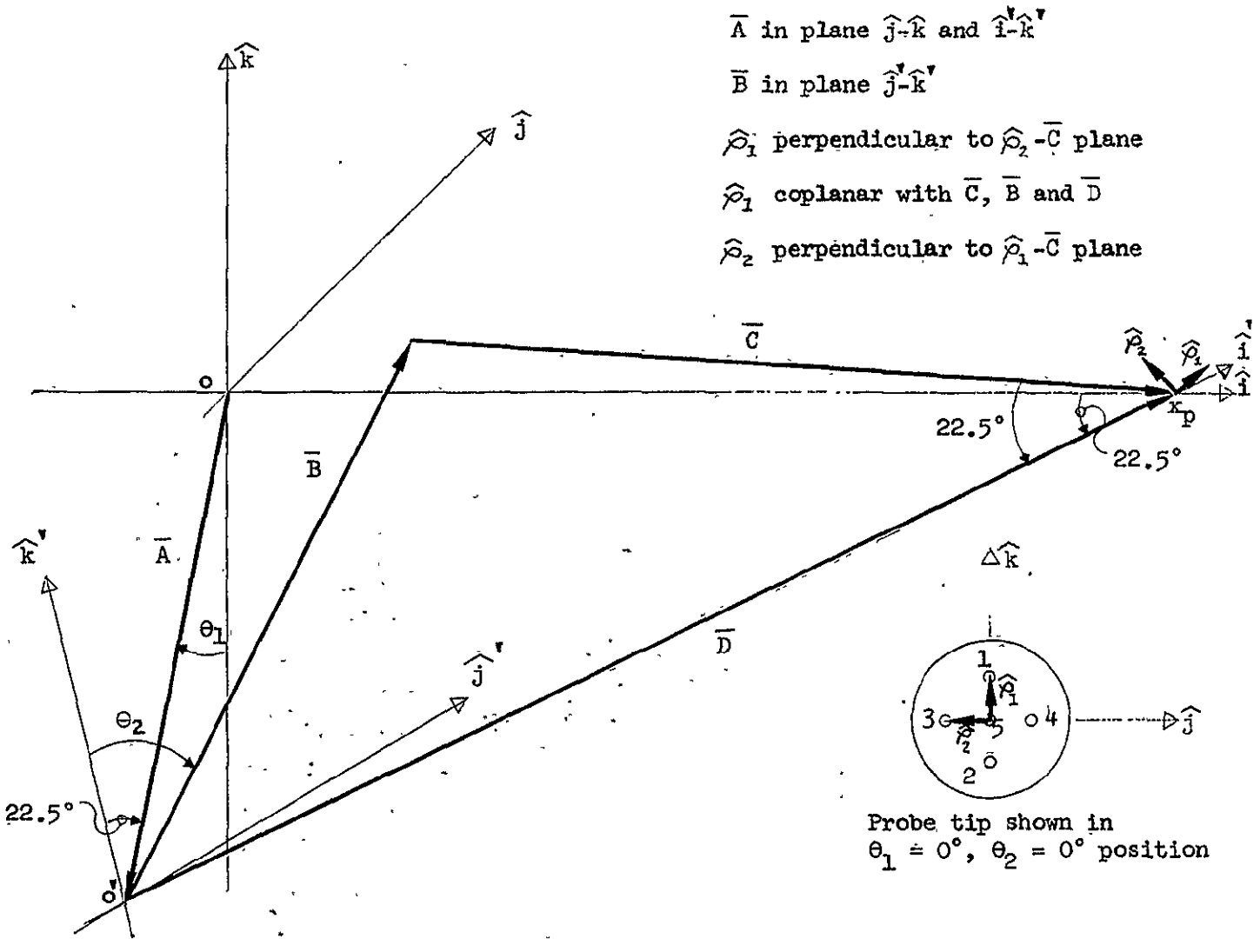

Figure 4. Vector relationship of probe parts.

angles are 0° for this orientation. Yaw right and pitch up of the sensing probe, with respect to axis 1, are considered as positive angles.

With $\theta_1 = 0^{\circ}$ and $\theta_2 = 0^{\circ}$ (see Figure 3) the following relations can be obtained:

$$\frac{B}{C} = \frac{A}{D} = \sin 22.5^{\circ} = 0.384 = m \tag{1}$$

$$\frac{A}{B} = \frac{D}{C} = \frac{x_p}{D} = \cos 22.5^{\circ} = 0.924 = n \tag{2}$$

It is necessary to define the vector $\overline{C}$, before yaw and pitch angle determinations can be made. When the probe has reached a null condition, this vector is colinear with the velocity vector. Referring to Figure 4, the relation between $\overline{C}$, $\overline{D}$, and $\overline{B}$ is

$$\overline{C} = \overline{D} - \overline{B} \tag{3}$$

and this can be expressed as

$$\hat{c} = \frac{\overline{C}}{C} = \frac{\overline{D}}{C} - \frac{\overline{B}}{C} \tag{4}$$

or

$$\hat{c} = \frac{D}{C}\hat{d} - \frac{B}{C}\hat{b} = n\hat{d} - m\hat{b} \tag{5}$$

Since

$$\hat{d} = \hat{i}' \tag{6}$$

and

$$\overline{B} = B \sin \theta_2 \, \hat{j}' + B \cos \theta_2 \, \hat{k}' \tag{7}$$

or

$$\hat{b} = \sin \theta_2 \, \hat{j}' + \cos \theta_2 \, \hat{k}' \tag{8}$$

then

$$\hat{c} = n \, \hat{i}' - m \sin \theta_2 \, \hat{j}' - m \cos \theta_2 \, \hat{k}' \tag{9}$$

The unit vectors $\hat{i}'$, $\hat{j}'$, and $\hat{k}'$ must now be expressed in terms of $\hat{i}$, $\hat{j}$, and $\hat{k}$. Again referring to Figure 4, it is seen that

$$\hat{i}' = \frac{\overline{D}}{|\overline{D}|} = \hat{d} \tag{10}$$

where

$$\overline{D} = x_p \, \hat{i} - \overline{A} \tag{11}$$

and

$$\overline{A} = - A \sin \theta_1 \, \hat{j} - A \cos \theta_1 \, \hat{k} \tag{12}$$

Then

$$\hat{i}' = \frac{x_p \, \hat{i} + A \sin \theta_1 \, \hat{j} + A \cos \theta_1 \, \hat{k}}{D} \tag{13}$$

Using the relations in equations (1) and (2),

$$\hat{i}' = n \, \hat{i} + m \sin \theta_1 \, \hat{j} + m \cos \theta_1 \, \hat{k} \tag{14}$$

If vector $\hat{j}'$ is perpendicular to the plane of $\hat{i}'$ and $\bar{A}$ ($\hat{i}'$, $\hat{k}'$, and $\bar{A}$ are always coplanar), then

$$\hat{j}' = \frac{\hat{i}' \times \hat{a}}{\left|\hat{i}' \times \hat{a}\right|} \tag{15}$$

where

$$\hat{a} = \frac{\bar{A}}{A} = -\sin\theta_1 \hat{j} - \cos\theta_1 \hat{k} \tag{16}$$

The cross product of $\hat{i}'$ and $\hat{a}$ can then be expressed as

$$\hat{i}' \times \hat{a} = \begin{vmatrix} \hat{i} & \hat{j} & \hat{k} \\ n & m\sin\theta_1 & m\cos\theta_1 \\ 0 & -\sin\theta_1 & -\cos\theta_1 \end{vmatrix} \tag{17}$$

which yields

$$\hat{i}' \times \hat{a} = n\cos\theta_1 \hat{j} - n\sin\theta_1 \hat{k} \tag{18}$$

The magnitude of the cross product is

$$\left|\hat{i}' \times \hat{a}\right| = \sin\angle(\hat{i}', \hat{a}) = \sin(90^\circ - 22.5^\circ) = \cos 22.5^\circ = n \tag{19}$$

Using the results of equations (18) and (19),

$$\hat{j}' = \frac{n\cos\theta_1 \hat{j} - n\sin\theta_1 \hat{k}}{n} \tag{20}$$

or

$$\hat{j}' = \cos\theta_1 \hat{j} - \sin\theta_1 \hat{k} \tag{21}$$

The remaining direction vector $\hat{k}'$ can be expressed as

$$\hat{k}' = \hat{i}' \times \hat{j}' \tag{22}$$

or

$$\hat{k}' = \begin{vmatrix} \hat{i} & \hat{j} & \hat{k} \\ n & m \sin\theta_1 & m \cos\theta_1 \\ 0 & \cos\theta_1 & -\sin\theta_1 \end{vmatrix} \tag{23}$$

Solving the determinant,

$$\hat{k}' = -m\,\hat{i} + n \sin\theta_1\,\hat{j} + n \cos\theta_1\,\hat{k} \tag{24}$$

Using this equation along with (14), (21) and (9), the unit vector $\hat{c}$ can be expressed as

$$\begin{aligned} \hat{c} = {} & n^2\,\hat{i} + mn \sin\theta_1\,\hat{j} + mn \cos\theta_1\,\hat{k} - m \sin\theta_2 \cos\theta_1\,\hat{j} \\ & + m \sin\theta_2 \sin\theta_1\,\hat{k} + m^2 \cos\theta_2\,\hat{i} - mn \sin\theta_1 \cos\theta_2\,\hat{j} \\ & - mn \cos\theta_1 \cos\theta_2\,\hat{k} \end{aligned} \tag{25}$$

Collecting terms,

$$\begin{aligned} \hat{c} = {} & (n^2 + m^2 \cos\theta_2)\hat{i} + (mn \sin\theta_1 - m \cos\theta_1 \sin\theta_2 \\ & - mn \sin\theta_1 \cos\theta_2)\hat{j} + (mn \cos\theta_1 + m \sin\theta_1 \sin\theta_2 \\ & - mn \cos\theta_1 \cos\theta_2)\hat{k} \end{aligned} \tag{26}$$

Since

$$\hat{c} = c_x\hat{i} + c_y\hat{j} + c_z\hat{k} \tag{27}$$

then

$$c_x = n^2 + m^2 \cos \theta_2 \tag{28}$$

$$c_y = mn \sin \theta_1 - m \cos \theta_1 \sin \theta_2 - mn \sin \theta_1 \cos \theta_2 \tag{29}$$

and

$$c_z = mn \cos \theta_1 + m \sin \theta_1 \sin \theta_2 - mn \cos \theta_1 \cos \theta_2 \tag{30}$$

The yaw and pitch angles can be determined using equations (28-30), since $\hat{c}$ represents the orientation of the probe. The angle of attack (pitch) is represented by α, and can be computed from the expression

$$\tan \alpha = \frac{c_z}{c_x} \quad \text{(pitch-up of the probe is positive)} \tag{31}$$

The angle of sideslip (yaw) is represented by ψ, and can be computed from the expression

$$\tan \psi = \frac{-c_y}{c_x} \quad \text{(yaw right of the probe is positive)} \tag{32}$$

Figure 5 shows locus plots of probe yaw and pitch angles for θ_1 and θ_2 values.

It is to be noted that, since the velocity vector has a heading directly opposite to that of the probe, the following relations exist:

1. Yaw right of the probe is equivalent to yaw right of the velocity vector.

2. Pitch up of the probe is equivalent to pitch down of the velocity vector.

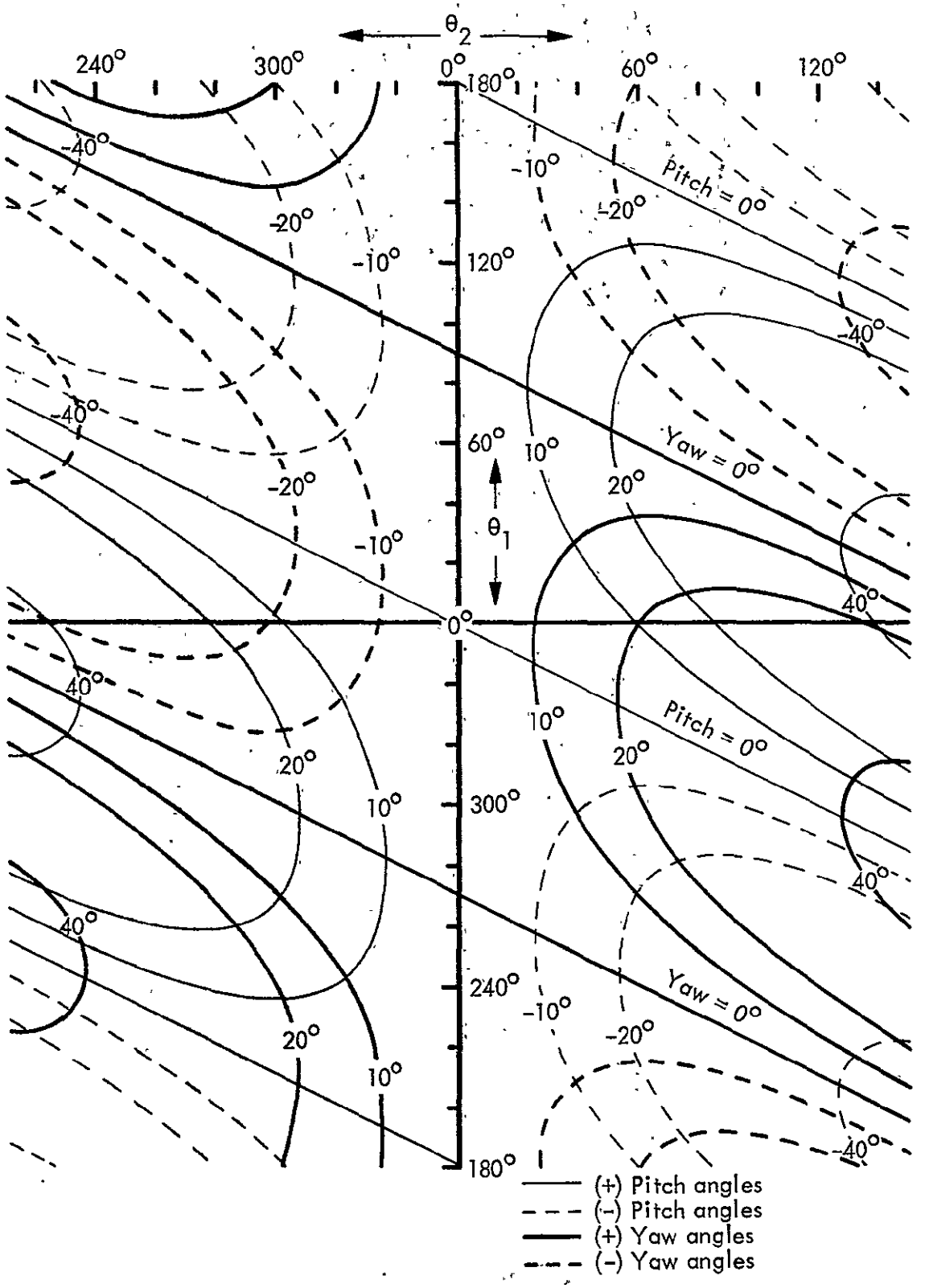

Figure 5. Yaw and pitch angle plots.

CHAPTER III

DESCRIPTION OF CONTROL SYSTEM

Manual and automatic control.--Figure 6 shows a schematic diagram of the basic control system used for the two angular motions that position the sensing probe. The only differences between the two systems are gain values in the servoamplifiers, gear reduction ratios, and pressure sensitivity to probe motions. Pressures picked up at the probe face are transmitted to transducers in the body of the probe. These transducers sense capacitance changes through motions of a stretched metal diaphram. The full range of the transducers is ±10 psid. They are so sensitive, however, that six other ranges are selectable by a switch on the signal conditioner. The most sensitive range is ±0.01 psid full scale. The signal conditioner provides amplification, so that a ±5 Vdc output is available on any of the ranges selected. This output is chopped and fed to a servoamplifier, the push-pull output of which is the control voltage for a two-phase servomotor. An a-c tachometer driven in tandem by the motor provides a damping signal back to the amplifier input. The motor drives its probe angular motion and a synchro transmitter through a high ratio gear reducer. The synchro provides a signal which is transmitted to a readout device used for monitoring and recording the angular position. This angular readout unit, located at the control chassis (see Figure 7), also contains the limit switches which prevent the probe from winding up and fouling its

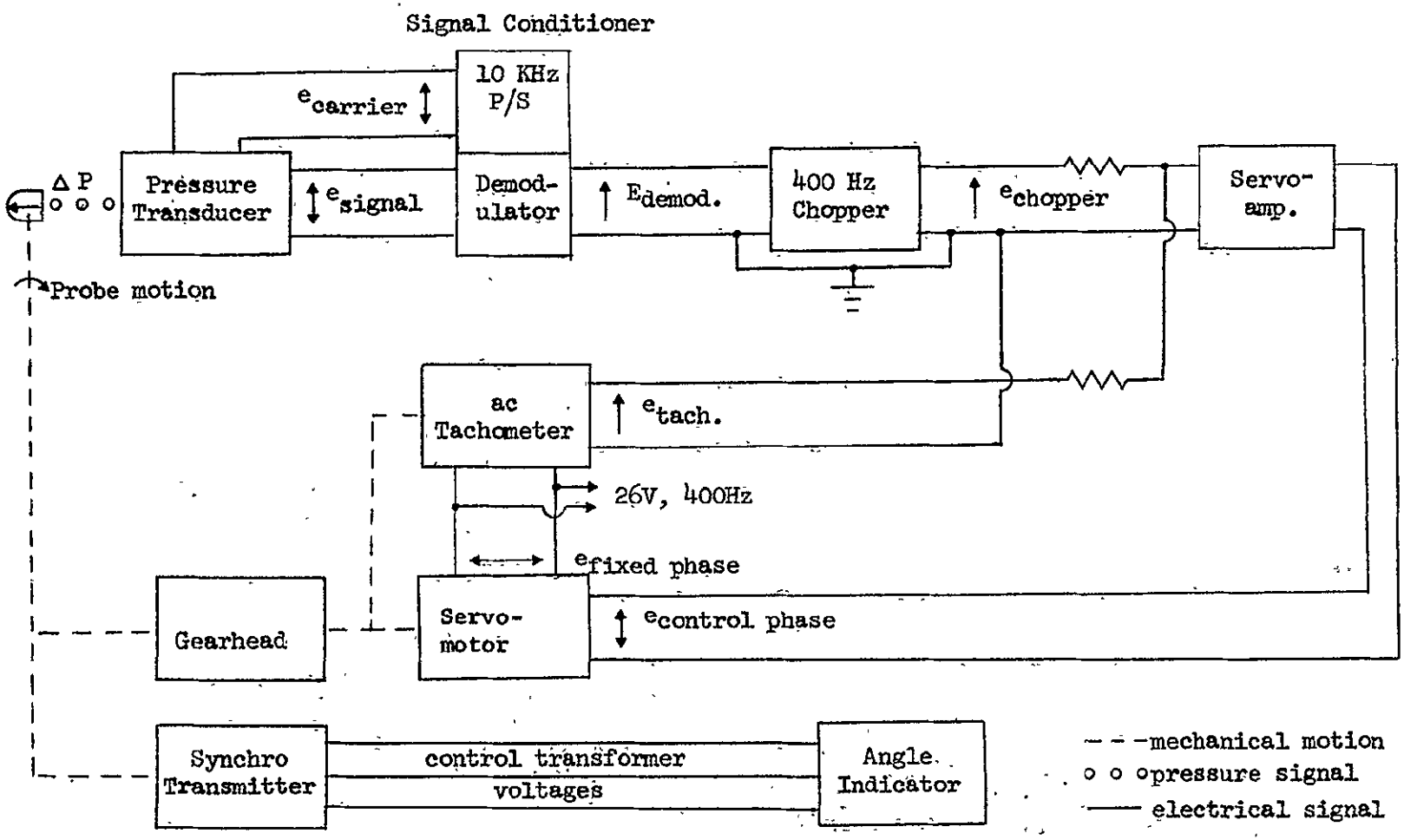

Figure 6. Basic control system schematic.

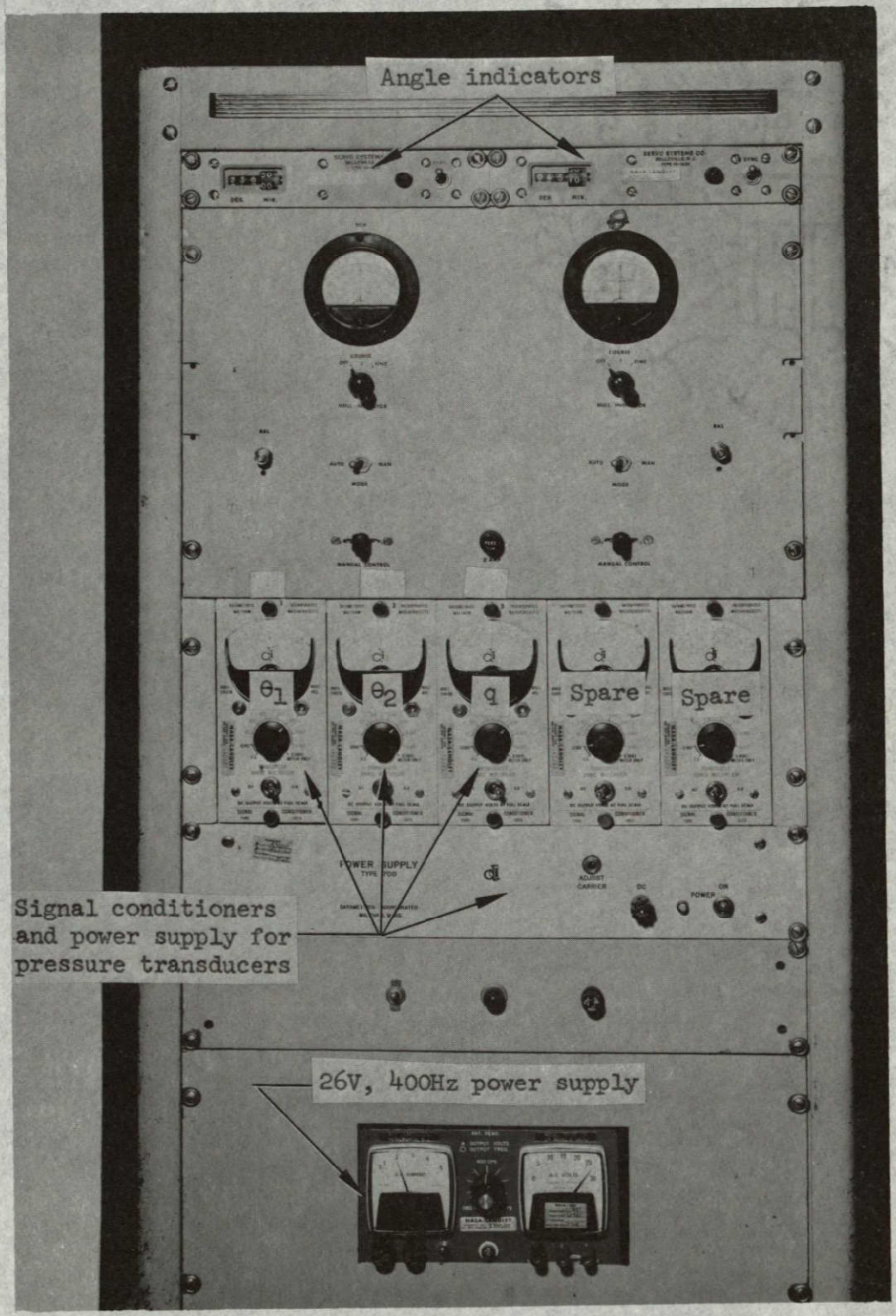

Figure 7. Control panel.

pressure lines and control wires. Space and wire limitations prevented the limit switches from being located within the probe itself.

Component description.- Brief comments on the probe parts follow:

A. ELECTRICAL COMPONENTS

(1) Pressure Transducers and Signal Conditioners - The pressure transducers used to sense the pressures at the ports on the probe face are located in the body of the probe's support axis (see Figure 2). These transducers employ stretched metal diaphrams, the motions of which are sensed as varying capacitance. This in turn modulates a 10 kHz carrier voltage which is supplied from a power supply located in the control panel. The signal conditioners (also located in the control panel) provide the necessary gain and demodulation circuits. Seven separate ranges or gain values may be selected by a switch on the signal conditioner. A ± 5 Vdc output is provided for the full scale value of each range. The selectable ranges are: ± 0.01 psid, ± 0.03 psid, ± 0.1 psid, ± 0.3 psid, ± 1.0 psid, ± 3.0 psid, and ± 10.0 psid.

(2) Servoamplifiers - The amplifiers used to drive the control motors are solid state devices capable of delivering 3.5 watts from a differential output. They are designed to drive the center tapped control winding of a two-phase 400 Hz servomotor. The gain can be set (up to 2500) by selection of an input resistor for single ended inputs.

(3) Servomotors, Generators and Gearheads - The control motor, feedback generator and gear reduction package are all integrated into one unit. Two units are provided and are identical with the exception of the gearheads. The θ_2 system has a 1446:1 gear reduction, and the

θ_1 system has a 496:1 gearhead with an additional 4:1 external reduction. The motors operate with a 26 V, 400 Hz fixed phase and a center tapped control winding. Their no-load speed is 6500 rpm. The generators also require 26 V, 400 Hz and deliver 0.11 V rms/1000 rpm for equivalent damping. These damping signals are summed (180° out of phase) with the control phase signal at the servoamplifiers, and the gains are set by selection of the input resistors.

(4) Choppers (400 Hz) - Solid state choppers driven at 400 Hz convert the dc output voltages from the pressure transducer signal conditioners to signals compatible with the 400 Hz servo components.

(5) Synchro Transmitters - The positions of the controlled angles are sensed by 400 Hz synchro transmitters. The synchros are located in the probe body, and are geared to the probe drive axes.

(6) Angle Indicators - The synchros in the probe are wired back to angle indicator units located in the control panel. The synchro transmitter signals are fed into control transformers. These control transformers are driven to a null by servomotors in the indicator units. Mechanical angle counters are geared to the servomotor-control transformer systems. Limit switches are also geared to this mechanical system. These limit switches are wired to limit the travel of the θ_1 and θ_2 motions on the probe.

(7) Control Chasis - The amplifiers, choppers, switches and relays used in controlling the servomotors are mounted on a chassis in the control panel (see Figure 7). This unit also contains meters for monitoring the pressures on the null ports.

B. MECHANICAL COMPONENTS

(1) Sensing Probe - The pitot type sensing probe was constructed from 0.1875 in. o.d. stainless steel tubing. Six smaller (0.020 in. i.d.) stainless steel tubes are contained inside the large tube. The hemispherical face of the probe contains the ports for five of the smaller tubes. The total pressure port is located on the probe axis. The nulling ports are separated by 90° on a plane perpendicular to the probe axis. Each is situated on the probe face at an angle of 45° to the probe axis. The static pressure ports are situated downstream from the probe face, and they feed the sixth small tube.

(2) Probe Body - The mounting assembly, the housings which contain the transducers, motors, generators, synchros and the drive trains were all designed at the National Aeronautics and Space Administration's Langley Research Center. The material used for the parts was stainless steel.

TABLE I

LIST OF COMPONENTS

Component	Manufacturer	Model number
Pressure transducer	Datametrics, Inc.	1055
Signal conditioner	Datametrics, Inc.	1015
Power supply	Datametrics, Inc.	700
400 Hz chopper	Solid State Electronics Corp.	64
Servoamplifier	Kearfott	C703148001
Servomotor-generator-gearhead	Clifton Precision Products	73750-AAY-1 and 73750-AAM-1
Synchro transmitter	Clifton Precision Products	CGH-8-F-7
Angle indicator	Servo Systems Co.	ED-1033 and ID-1034
Sensing Probe, Housings and Support Section	NASA-LRC	---

Manual control.- The drive mode for the probe motions is selected by a switch located on the control chassis. When it is desired to position the probe manually, the input to the chopper is switched from the transducer signal conditioner output to a battery and polarity switching network. The probe can be manually driven to a null by observing the metered outputs of the pressure transducers.

Automatic control.- As previously stated, there are two angular motions (θ_1 and θ_2) employed in positioning the probe to its proper null point. The motors controlling these motions are driven by error signals obtained from differential pressure transducers and their signal conditioners. One pressure transducer senses the pressure between ports 1 and 2 (P_{1-2}), and another senses the pressure between ports 3 and 4 (P_{3-4}).

At first, it was thought that it would make little difference which error signal was used to drive the motor controlling θ_2. However, when θ_2 is controlled by the pressure difference signal at ports 1 and 2, the system is unstable. This can be demonstrated by the following mathematical analysis:

Referring to Figure 4,

(1) The unit vector $\hat{\rho}_1$ defines the orientation of a line which passes through point x_p and is parallel to a line between ports 1 and 2 (the direction of $\hat{\rho}_1$ is from port 2 to port 1).

(2) The unit vector $\hat{\rho}_2$ defines the orientation of ports 3 and 4 in a like manner (the direction of $\hat{\rho}_2$ is from port 4 to port 3).

The vectors $\hat{\rho}_1$ and $\hat{\rho}_2$ can be defined in terms of θ_1 and θ_2 as follows:

From Figure 4 it can be seen that

$$\hat{\rho}_2 = \hat{i}' \times \hat{b} \tag{33}$$

Using equation (8),

$$\hat{\rho}_2 = \hat{i}' \times (\sin \theta_2 \, \hat{j}' + \cos \theta_2 \, \hat{k}') \tag{34}$$

or

$$\hat{\rho}_2 = - \cos \theta_2 \, \hat{j}' + \sin \theta_2 \, \hat{k}' \tag{35}$$

Using equations (21) and (23),

$$\begin{aligned} \hat{\rho}_2 = & - \cos \theta_2 (\cos \theta_1 \, \hat{j} - \sin \theta_1 \, \hat{k}) \\ & + \sin \theta_2 (- m \, \hat{i} + n \sin \theta_1 \, \hat{j} + n \cos \theta_1 \, \hat{k}) \end{aligned} \tag{36}$$

and finally

$$\begin{aligned} \hat{\rho}_2 = & - m \sin \theta_2 \, \hat{i} + (n \sin \theta_1 \sin \theta_2 - \cos \theta_1 \cos \theta_2) \hat{j} \\ & + (n \cos \theta_1 \sin \theta_2 + \sin \theta_1 \cos \theta_2) \hat{k} \end{aligned} \tag{37}$$

Vector $\hat{\rho}_1$ can be expressed as

$$\hat{\rho}_1 = \hat{\rho}_2 \times \hat{c} \tag{38}$$

Using equations (35) and (9)

$$\hat{\rho}_1 = \begin{vmatrix} \hat{i}' & \hat{j}' & \hat{k}' \\ 0 & -\cos\theta_2 & \sin\theta_2 \\ n & -m\sin\theta_2 & -m\cos\theta_2 \end{vmatrix} \tag{39}$$

Solving the determinant,

$$\hat{\rho}_1 = (m\cos^2\theta_2 + m\sin^2\theta_2)\hat{i}' + n\sin\theta_2\,\hat{j}' + n\cos\theta_2\,\hat{k}' \tag{40}$$

Using equations (14), (21), and (24),

$$\begin{aligned} \hat{\rho}_1 = {} & m(n\,\hat{i} + m\sin\theta_1\,\hat{j} + m\cos\theta_1\,\hat{k}) \\ & + n\sin\theta_2(\cos\theta_1\,\hat{j} - \sin\theta_1\,\hat{k}) \\ & + n\cos\theta_2(-m\,\hat{i} + n\sin\theta_1\,\hat{j} + n\cos\theta_1\,\hat{k}) \end{aligned} \tag{41}$$

Combining terms,

$$\begin{aligned} \hat{\rho}_1 = {} & (mn - mn\cos\theta_2)\hat{i} + (m^2\sin\theta_1 + n\cos\theta_1\sin\theta_2 \\ & + n^2\sin\theta_1\cos\theta_2)\hat{j} + (m^2\cos\theta_1 - n\sin\theta_1\sin\theta_2 \\ & + n^2\cos\theta_1\cos\theta_2)\hat{k} \end{aligned} \tag{42}$$

This defines $\hat{\rho}_1$, a unit vector which can be used to represent the orientation of ports 1 and 2. Likewise, $\hat{\rho}_2$ represents the orientation of ports 3 and 4. The relationship of $\hat{\rho}_1$ and $\hat{\rho}_2$ to the velocity vector is now developed.

Let $\hat{v}$ = unit vector representing the orientation of wind velocity. For this analysis, assume that $\hat{v}$ is constant and only the probe can move. At a null,

$$\hat{v} = -\hat{c} \qquad (\hat{c} = \text{unit vector along the pitot probe axis}) \tag{43}$$

and

$$\hat{v} \cdot \hat{\rho}_1 = \hat{v} \cdot \hat{\rho}_2 = 0 \tag{44}$$

For small angular deviations, the pressure differences between ports 1 and 2 will be directly proportional to the amount that the angle between $\hat{\rho}_1$ and $\hat{v}$ differs from 90°. The same holds for the pressure difference between ports 3 and 4 and the angle between $\hat{\rho}_2$ and $\hat{v}$. This was shown by empirical testing of the hemispherical probe (see Appendix I). The relation was found to be

$$\frac{P_{1-2}}{\phi_1} = \frac{P_{3-4}}{\phi_2} = 0.07\ q(\text{psi})/\text{deg} \tag{45}$$

And q, ϕ_1, and ϕ_2 are defined as follows:

q = dynamic pressure in psi

ϕ_1 = angular deviation of $\hat{\rho}_1$ and $\hat{v}$ from orthogonality

ϕ_2 = angular deviation of $\hat{\rho}_2$ and $\hat{v}$ from orthogonality

The dot products of $\hat{v}$ with $\hat{\rho}_1$ and $\hat{\rho}_2$ can be expressed as

$$\hat{v} \cdot \hat{\rho}_1 = |\hat{v}||\hat{\rho}_1| \cos (90^\circ \pm \phi_1) \tag{46}$$

and

$$\hat{v} \cdot \hat{\rho}_2 = |\hat{v}||\hat{\rho}_2| \cos (90^\circ \pm \phi_2) \tag{47}$$

Since

$$|\hat{v}| = |\hat{\rho}_1| = |\hat{\rho}_2| = 1 \tag{48}$$

these expressions reduce to

$$\hat{v} \cdot \hat{\rho}_1 = \cos (90^\circ \pm \phi_1) = \mp \sin \phi_1 \approx \mp \phi_1 \tag{49}$$

and

$$\hat{v} \cdot \hat{\rho}_2 = \cos (90^\circ \pm \phi_2) = \mp \sin \phi_2 \approx \mp \phi_2 \tag{50}$$

for small values of ϕ_1 and ϕ_2.

Determination of control motion sensitivities.- By determining $\frac{\partial(\hat{v} \cdot \hat{\rho}_1)}{\partial\theta_1} \approx \frac{\partial\phi_1}{\partial\theta_1}$, $\frac{\partial(\hat{v} \cdot \hat{\rho}_2)}{\partial\theta_2} \approx \frac{\partial\phi_2}{\partial\theta_2}$, $\frac{\partial(\hat{v} \cdot \hat{\rho}_1)}{\partial\theta_2} \approx \frac{\partial\phi_1}{\partial\theta_2}$, and $\frac{\partial(\hat{v} \cdot \hat{\rho}_2)}{\partial\theta_1} \approx \frac{\partial\phi_2}{\partial\theta_1}$ (Refs. 13 and 14) the effect on pressure differences between ports 1 and 2, and ports 3 and 4 by θ_1 and θ_2 motions can be found. At any given null condition, $\hat{v} = -\hat{c}$, and θ_1 and θ_2 are at some fixed positions, θ_1' and θ_2'. The velocity vector can then be described from equation (26) as

$$\begin{aligned}\hat{v} = {} & (-n^2 - m^2 \cos\theta_2')\hat{i} + (-mn \sin\theta_1' + m \cos\theta_1' \sin\theta_2' \\ & + mn \sin\theta_1' \cos\theta_2')\hat{j} + (-mn \cos\theta_1' - m \sin\theta_1' \sin\theta_2' \\ & + mn \cos\theta_1' \cos\theta_2')\hat{k}\end{aligned} \tag{51}$$

The effect of θ_2 on P_{1-2} can be found from

$$\begin{aligned}\frac{\partial(\hat{v} \cdot \hat{\rho}_1)}{\partial\theta_2} = {} & \rho_{1x}\left(\frac{\partial v_x}{\partial\theta_2}\right) + v_x\left(\frac{\partial\rho_{1x}}{\partial\theta_2}\right) + \rho_{1y}\left(\frac{\partial v_y}{\partial\theta_2}\right) + v_y\left(\frac{\partial\rho_{1y}}{\partial\theta_2}\right) \\ & + \rho_{1z}\left(\frac{\partial v_z}{\partial\theta_2}\right) + v_z\left(\frac{\partial\rho_{1z}}{\partial\theta_2}\right)\end{aligned} \tag{52}$$

Since $\hat{v}$ is considered constant

$$\frac{\partial v_x}{\partial \theta_2} = \frac{\partial v_y}{\partial \theta_2} = \frac{\partial v_z}{\partial \theta_2} = 0 \tag{53}$$

and the equation simplifies to

$$\frac{\partial(\hat{v} \cdot \hat{\rho}_1)}{\partial \theta_2} = v_x\left(\frac{\partial \rho_{1x}}{\partial \theta_2}\right) + v_y\left(\frac{\partial \rho_{1y}}{\partial \theta_2}\right) + v_z\left(\frac{\partial \rho_{1z}}{\partial \theta_2}\right) \tag{54}$$

The terms v_x, v_y, and v_z can be obtained from equation (51), and ρ_{1x}, ρ_{1y}, and ρ_{1z} from (42). Then after determining $\frac{\partial \rho_{1x}}{\partial \theta_2}$, $\frac{\partial \rho_{1y}}{\partial \theta_2}$, and $\frac{\partial \rho_{1z}}{\partial \theta_2}$ the effect on P_{1-2} by θ_2 at some null point can be expressed as

$$\left.\frac{\partial(\hat{v} \cdot \hat{\rho}_1)}{\partial \theta_2}\right|_{\substack{\theta_1 = \theta_1' \\ \theta_2 = \theta_2'}} = (-n^2 - m^2 \cos\theta_2')(mn \sin\theta_2')$$
$$+ (-mn \sin\theta_1' + m \cos\theta_1' \sin\theta_2' + mn \sin\theta_1' \cos\theta_2')$$
$$(n \cos\theta_1' \cos\theta_2' - n^2 \sin\theta_1' \sin\theta_2')$$
$$+ (-mn \cos\theta_1' - m \sin\theta_1' \sin\theta_2' + mn \cos\theta_1' \cos\theta_2')$$
$$(-n \sin\theta_1' \cos\theta_2' - n^2 \cos\theta_1' \sin\theta_2') \tag{55}$$

Multiplying terms and simplifying,

$$\left.\frac{\partial(\hat{v} \cdot \hat{\rho}_1)}{\partial \theta_2}\right|_{\substack{\theta_1 = \theta_1' \\ \theta_2 = \theta_2'}} = mn \sin\theta_2' \cos\theta_2' \left[1 - (m^2 + n^2)\right] = 0 \tag{56}$$

Since P_{1-2} is proportional to $\hat{v} \cdot \hat{\rho}_1$, then $\frac{\Delta P_{1-2}}{\Delta \theta_2}$ is also zero. This means that P_{1-2} will not change for small changes in θ_2 from its null position. By examining the function $\frac{\partial(\hat{v} \cdot \hat{\rho}_1)}{\partial \theta_2}$ at values of

$$\theta_2 = \theta_2' + \theta_{\epsilon 2} \qquad (\theta_{\epsilon 2} = \text{small angular change})$$

and

$$\theta_2 = \theta_2' - \theta_{\epsilon 2}$$

it can be seen that $\frac{\partial(\hat{v} \cdot \hat{\rho}_1)}{\partial \theta_2} = 0$ at null conditions because a maximum exists. This results in a condition of instability. The error signals due to P_{1-2} must be opposite in sign on each side of the null point. This is not possible if a maximum exists.

Since θ_2 cannot be controlled by pressures at ports 1 and 2, $\frac{\partial(\hat{v} \cdot \hat{\rho}_2)}{\partial \theta_2}$ must be examined. This relation can be expressed as

$$\frac{\partial(\hat{v} \cdot \hat{\rho}_2)}{\partial \theta_2} = \rho_{2x}\left(\frac{\partial v_x}{\partial \theta_2}\right) + v_x\left(\frac{\partial \rho_{2x}}{\partial \theta_2}\right) + \rho_{2y}\left(\frac{\partial v_y}{\partial \theta_2}\right) + v_y\left(\frac{\partial \rho_{2y}}{\partial \theta_2}\right) + \rho_{2z}\left(\frac{\partial v_z}{\partial \theta_2}\right) + v_z\left(\frac{\partial \rho_{2z}}{\partial \theta_2}\right) \tag{57}$$

And since

$$\frac{\partial v_x}{\partial \theta_2} = \frac{\partial v_y}{\partial \theta_2} = \frac{\partial v_z}{\partial \theta_2} = 0, \tag{58}$$

then

$$\frac{\partial(\hat{v} \cdot \hat{\rho}_2)}{\partial\theta_2} = v_x\left(\frac{\partial\rho_{2x}}{\partial\theta_2}\right) + v_y\left(\frac{\partial\rho_{2y}}{\partial\theta_2}\right) + v_z\left(\frac{\partial\rho_{2z}}{\partial\theta_2}\right) \tag{59}$$

Once again v_x, v_y, and v_z are obtained from equation (51), but ρ_{2x}, ρ_{2y}, and ρ_{2z} are found in (37). After determining $\frac{\partial\rho_{2x}}{\partial\theta_2}$, $\frac{\partial\rho_{2y}}{\partial\theta_2}$, and $\frac{\partial\rho_{2z}}{\partial\theta_2}$, the effect on P_{3-4} by θ_2 motions at some null point can be expressed as

$$\begin{aligned}\left.\frac{\partial(\hat{v} \cdot \hat{\rho}_2)}{\partial\theta_2}\right|_{\substack{\theta_1 = \theta_1' \\ \theta_2 = \theta_2'}} &= (-n^2 - m^2\cos\theta_2')(-m\cos\theta_2') \\ &\quad + (-mn\sin\theta_1' + m\cos\theta_1'\sin\theta_2' + mn\sin\theta_1'\cos\theta_2') \\ &\qquad (n\sin\theta_1'\cos\theta_2' + \cos\theta_1'\sin\theta_2') \\ &\quad + (-mn\cos\theta_1' - m\sin\theta_1'\sin\theta_2' + mn\cos\theta_1'\cos\theta_2') \\ &\qquad (n\cos\theta_1'\cos\theta_2' - \sin\theta_1'\sin\theta_2')\end{aligned} \tag{60}$$

Multiplying terms and simplifying,

$$\left.\frac{\partial(\hat{v} \cdot \hat{\rho}_2)}{\partial\theta_2}\right|_{\substack{\theta_1 = \theta_1' \\ \theta_2 = \theta_2'}} = m \tag{61}$$

This result shows that for small changes in θ_2 about a null position, P_{3-4} will be directly proportional to changes in θ_2. It also shows that the sensitivity is independent of the null position (θ_1', θ_2').

This analysis has shown that the motor driving θ_2 must be controlled by error signals due to pressure differences between ports 3 and 4. That leaves θ_1 to be controlled by pressure differences between ports 1 and 2. The sensitivity of P_{1-2} to θ_1 motions can be determined from

$$\frac{\partial(\hat{v} \cdot \hat{\rho}_1)}{\partial\theta_1} = \rho_{1x}\left(\frac{\partial v_x}{\partial\theta_1}\right) + v_x\left(\frac{\partial\rho_{1x}}{\partial\theta_1}\right) + \rho_{1y}\left(\frac{\partial v_y}{\partial\theta_1}\right) + v_y\left(\frac{\partial\rho_{1y}}{\partial\theta_1}\right) + \rho_{1z}\left(\frac{\partial v_z}{\partial\theta_1}\right) + v_z\left(\frac{\partial\rho_{1z}}{\partial\theta_1}\right) \tag{62}$$

Since

$$\frac{\partial v_x}{\partial\theta_1} = \frac{\partial v_y}{\partial\theta_1} = \frac{\partial v_z}{\partial\theta_1} = 0 \tag{63}$$

and

$$\frac{\partial\rho_{1x}}{\partial\theta_1} = 0, \text{ since } \rho_{1x} \neq f(\theta_1) \tag{64}$$

then

$$\frac{\partial(\hat{v} \cdot \hat{\rho}_1)}{\partial\theta_1} = v_y\left(\frac{\partial\rho_{1y}}{\partial\theta_1}\right) + v_z\left(\frac{\partial\rho_{1z}}{\partial\theta_1}\right) \tag{65}$$

The terms v_y and v_z are obtained from equation (51), and ρ_{1y} and ρ_{1z} from (42). After finding $\frac{\partial\rho_{1y}}{\partial\theta_1}$ and $\frac{\partial\rho_{1z}}{\partial\theta_1}$, the effect on P_{1-2} due to θ_1 motions at some null point can be expressed as

$$\left.\frac{\partial(\hat{v} \cdot \hat{\rho}_1)}{\partial\theta_1}\right|_{\substack{\theta_1 = \theta_1' \\ \theta_2 = \theta_2'}} = (-mn \sin\theta_1' + m\cos\theta_1' \sin\theta_2' + mn \sin\theta_1' \cos\theta_2')$$
$$(m^2 \cos\theta_1' - n \sin\theta_1' \sin\theta_2' + n^2 \cos\theta_1' \cos\theta_2')$$
$$+ (-mn \cos\theta_1' - m \sin\theta_1' \sin\theta_2' + mn \cos\theta_1' \cos\theta_2')$$
$$(-m^2 \sin\theta_1' - n \cos\theta_1' \sin\theta_2' - n^2 \sin\theta_1' \cos\theta_2') \tag{66}$$

Multiplying and simplifying,

$$\left.\frac{\partial(\hat{v} \cdot \hat{\rho}_1)}{\partial\theta_1}\right|_{\substack{\theta_1 = \theta_1' \\ \theta_2 = \theta_2'}} = m \sin\theta_2' \tag{67}$$

The following is revealed about changes in P_{1-2} for small changes in θ_1 about a null position:

(1) The magnitude and sign of the change are dependent on the probe's null position due to the $\sin\theta_2'$ term.

(2) There are no pressure variations when $\theta_2' = 0^\circ, 180^\circ$.

It has been previously shown by equation (56) that the pressure between ports 1 and 2 is not disturbed by small changes in θ_2 about the null point. It will be of interest to determine the disturbance on the pressure between ports 3 and 4 due to changes in θ_1. This determination is made by finding $\frac{\partial(\hat{v} \cdot \hat{\rho}_2)}{\partial\theta_1}$ which can be expressed as

$$\frac{\partial(\hat{v} \cdot \hat{\rho}_2)}{\partial\theta_1} = \rho_{2x}\left(\frac{\partial v_x}{\partial\theta_1}\right) + v_x\left(\frac{\partial\rho_{2x}}{\partial\theta_1}\right) + \rho_{2y}\left(\frac{\partial v_y}{\partial\theta_1}\right) + v_y\left(\frac{\partial\rho_{2y}}{\partial\theta_1}\right)$$
$$+ \rho_{2z}\left(\frac{\partial v_z}{\partial\theta_1}\right) + v_z\left(\frac{\partial\rho_{2z}}{\partial\theta_1}\right) \tag{68}$$

The velocity vector ($\hat{v}$) is constant, and thus,

$$\frac{\partial v_x}{\partial \theta_1} = \frac{\partial v_y}{\partial \theta_1} = \frac{\partial v_z}{\partial \theta_1} = 0 \tag{69}$$

Since $\rho_{1x} \neq f(\theta_1)$,

$$\frac{\partial \rho_{2x}}{\partial \theta_1} = 0 \tag{70}$$

and equation (68) reduces to

$$\frac{\partial(\hat{v} \cdot \hat{\rho}_2)}{\partial \theta_1} = v_y\left(\frac{\partial \rho_{2y}}{\partial \theta_1}\right) + v_z\left(\frac{\partial \rho_{2z}}{\partial \theta_1}\right) \tag{71}$$

Terms v_y and v_z are obtained from equation (51), and ρ_{2y} and ρ_{2z} from (37). After finding $\frac{\partial \rho_{2y}}{\partial \theta_1}$ and $\frac{\partial \rho_{2z}}{\partial \theta_1}$

$$\left.\frac{\partial(\hat{v} \cdot \hat{\rho}_2)}{\partial \theta_1}\right|_{\substack{\theta_1 = \theta_1' \\ \theta_2 = \theta_2'}} = (-mn \sin\theta_1' + m\cos\theta_1' \sin\theta_2' + mn \sin\theta_1' \cos\theta_2')$$
$$(n\cos\theta_1' \sin\theta_2' + \sin\theta_1' \cos\theta_2')$$
$$+ (-mn\cos\theta_1' - m\sin\theta_1' \sin\theta_2' + mn\cos\theta_1' \cos\theta_2')$$
$$(-n\sin\theta_1' \sin\theta_2' + \cos\theta_1' \cos\theta_2') \tag{72}$$

Multiplying and simplifying,

$$\left.\frac{\partial(\hat{v} \cdot \hat{\rho}_2)}{\partial \theta_1}\right|_{\substack{\theta_1 = \theta_1' \\ \theta_2 = \theta_2'}} = mn(1 - \cos\theta_2') \tag{73}$$

The following is revealed about changes in P_{3-4} for small changes in θ_1 from its null position:

(1) The change is dependent on the probe's null position due to the term $(\cos \theta_2')$

(2) The sensitivity is greatest at $\theta_2' = 180^\circ$ and is zero at $\theta_2' = 0^\circ$.

From this analysis it was found that there is a disturbance on the servosystem which controls θ_2 due to the interaction caused by θ_1 motions. However, the converse is not true. Motions of θ_2 (near the null condition) do not affect the servosystem controlling θ_1.

CHAPTER IV

ANALYSIS OF CONTROL SYSTEMS

System equations and block diagrams.- For any given velocity vector within the range of the probe there is a set of yaw and pitch angles which identifies its heading. These yaw and pitch angles are achieved through control motion settings of θ_1' and θ_2'. These angles (θ_1' and θ_2') are the reference inputs to the two feedback control systems. A block diagram showing the two control systems and their interactions for small signal analysis is shown in Figure 8.

The blocks $G_1'(S)$ and $G_2'(S)$ represent the cascade transfer functions of inner loops. Each of these loops is made up of an amplifier, a motor and a feedback generator. The block diagram for this inner loop is shown in Figure 9. The development of the transform $G'(S)$ is given in Appendix II (Ref. 15).

Each of the systems can be considered a simple positioning servomechanism by combining the cascade blocks and moving the disturbance outside the loop (ref. 16). Figure 10 is a generalized block diagram of such a system. A new reference (R') is formed by the effect of the disturbance input. The transfer function for this system would be:

$$\frac{\theta(S)}{R'(S)} = \frac{K_T}{S\left(S + \frac{h + kk_e k_g}{J}\right)(S + \gamma) + K_T} \qquad (74)$$

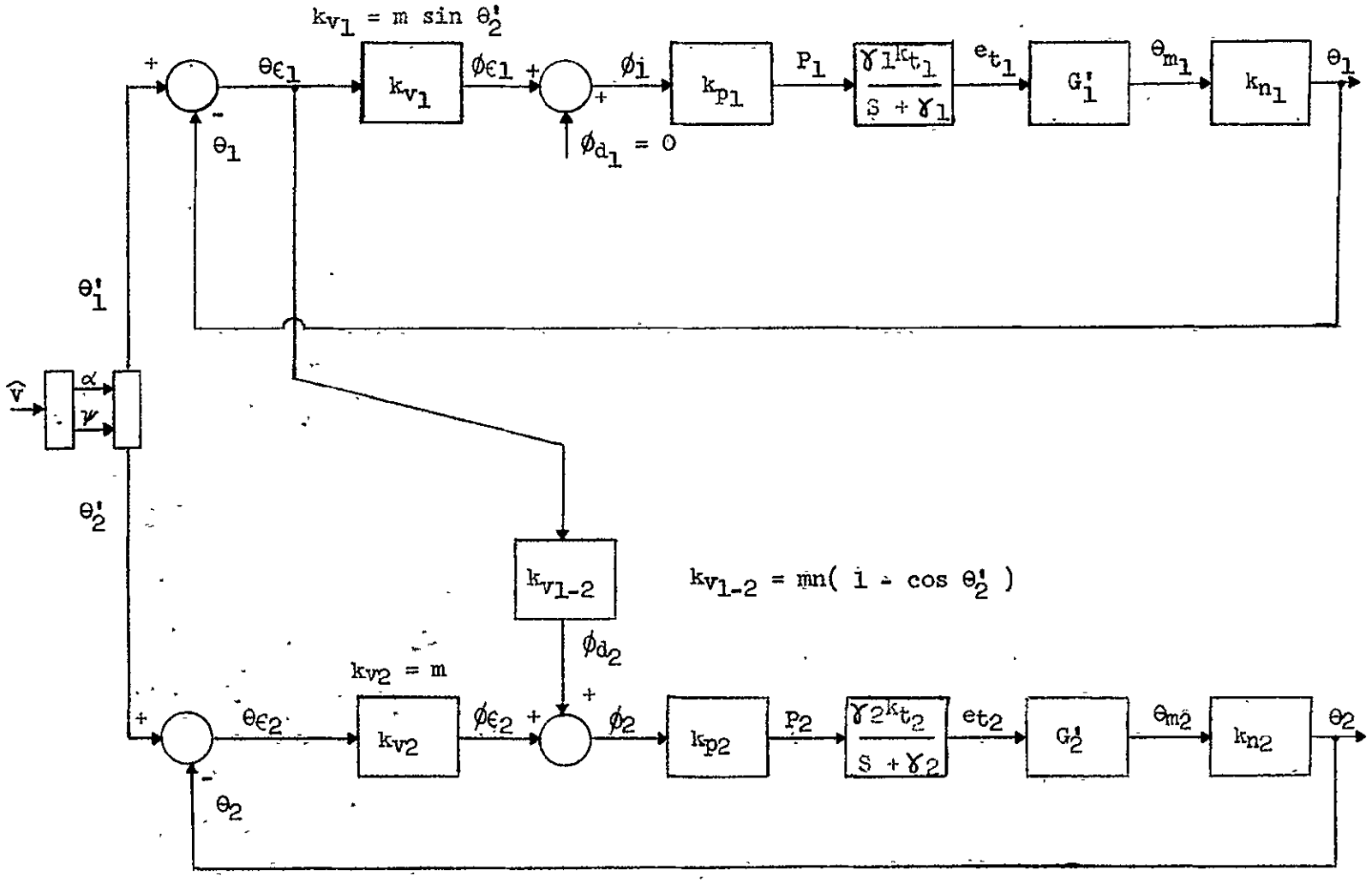

Figure 8. Block diagram of control system.

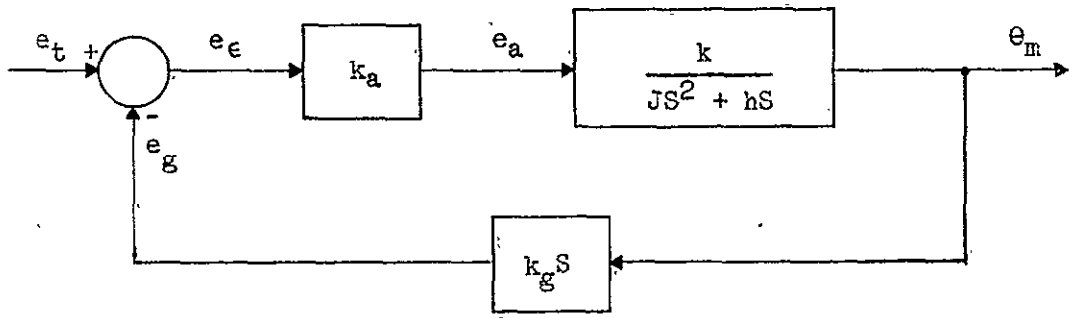

$$\theta_m = G'(S)e_t$$

$$G'(S) = \frac{\frac{kk_a}{J}}{S(S + \frac{h + kk_ak_g}{J})}$$

Figure 9. Block diagram of inner loop.

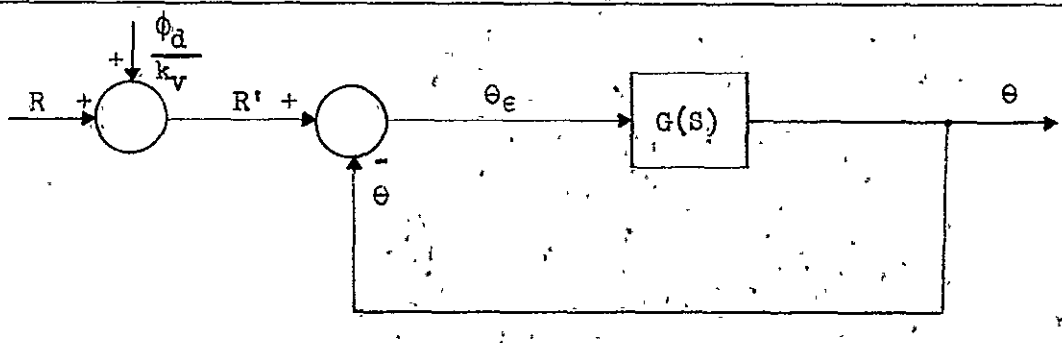

$$G(S) = \frac{K_T}{S(S + \frac{h + kk_ak_g}{J})(S + \gamma)}$$

$$K_T = \frac{k_v k_p k_t k k_a k_n \gamma}{J}$$

Figure 10. Generalized block diagram.

where,

$$K_T = \frac{k_v k_p k_t k k_a k_n \gamma}{J} \tag{75}$$

Discussion of the control systems.- The forward loop gain as taken from Figure 10 is

$$G(S) = \frac{K_T}{S\left(S + \frac{h + k k_a k_g}{J}\right)(S + \gamma)} \tag{76}$$

This can be expressed in terms of the velocity constant K_V and the equivalent time constant τ as

$$G(S) = \frac{\frac{K_V \gamma}{\tau}}{S\left(S + \frac{1}{\tau}\right)(S + \gamma)} \tag{77}$$

where

$$K_V = \frac{K_T}{\left(\frac{h + k k_a k_g}{J}\right)\gamma} \tag{78}$$

and

$$\tau = \frac{J}{h + k k_a k_g} \tag{79}$$

Since the system has unity feedback, $G(S)$ is also the open-loop transfer function. The single pole at the origin makes this a type 1 system. Theoretically, type 1 systems have no steady state errors for a step input. This is desirable in a null seeking system such as this.

It was not necessary to design for a low velocity error, because the probe is to be used for making static interrogations of points in a wind tunnel. In using the probe, turbulent conditions will often be encountered. To filter out the effects of these noise signals, the system's variable constants can be adjusted to make the system a low pass filter. Also a large damping factor is necessary, since the angle indicator unit has a limited slewing speed. If turbulence is not a problem, and if a faster responding angle indicator were used (all electronic), the response of the system could be improved. Increasing the gain, using phase lead compensation, or a combination of both, would accomplish this. There is considerable gain margin in each of the systems. This is illustrated in the root locus plots which are developed in Appendix III.

θ_1 system.- From Figure 8 it is obvious that while the θ_1 system has no direct disturbances from the θ_2 system at a null condition, it is affected by the θ_2 system. This is due to the fact that the term $\sin \theta_2'$ appears in the k_{v_1} transfer function. Two problems are immediately evident. First, a condition of instability will occur if θ_2' is allowed to take on negative values. Secondly, the system becomes an open loop when $\theta_2' = 0^\circ$. The first problem was solved by limiting θ_2' to positive values by setting the limit switches at: $\theta_2 = 0^\circ$ and $\theta_2 = 178^\circ$. This does not compromise the probe's range of yaw and pitch angles. As can be seen in Figure 5, there are two null points for each combination of yaw and pitch angles within the probe's range. One null point is in the negative θ_2' range, and one is in the

positive range. The second problem occurs only when $\theta_2' = 0^\circ$. It is true that θ_1 is subject to random drifting when this occurs. However, when $\theta_2 = 0^\circ$, the special condition exists that yaw and pitch angles are both equal to zero. In this special condition θ_1 can assume any position without loss of accuracy. This can be seen by again examining Figure 5.

θ_2 system.- This system has no position dependent transfer functions within the closed loop. However, it is subject to disturbances from the θ_1 system. These disturbance signals are dependent on the position of θ_2 due to the term $\cos \theta_2'$ in the disturbance transfer function (see Figure 8). It is most fortunate that when θ_1 tends to drift ($\theta_2 = 0^\circ$), the transfer function for its disturbing effects on θ_2 takes on a value of zero.

CHAPTER V

EXPERIMENTAL RESULTS AND CONCLUSIONS

Wind tunnel and lab tests.- Calibration tests were made on the probe at Langley's 7 × 10-foot research facility model tunnel. These tests showed the probe to have yaw and pitch angle errors of up to 2.5°. The repeatability of the probe, however, was better than 0.2°. The errors seemed to be systematic, so further tests were made with the probe in the laboratory. The results of these tests showed that the errors were due to two things:

(1) Deadband in the θ_1 drive gears of nearly 2°.

(2) Misalignment of the nulling ports.

Both $\hat{\rho}_1$ and $\hat{\rho}_2$ have apparent deviations of 0.75° from the ideal condition of orthogonality with the probe axis. The word "apparent" is used, since the condition could be caused by other factors such as an uneven pressure profile on the probe's face.

Recommendations and concluding remarks.- The deadband that was found in the θ_1 system was removed by making some mechanical improvements on a gear key. The misalignment of the nulling ports can be compensated for by setting an offset voltage on the signal conditioners for the null pressure transducers. The level of the offset will be dependent on the tunnel dynamic pressure (q). The probe is presently waiting access to the model tunnel for further calibration tests. Even if the above corrections do not bring the absolute error to within 1° it is felt that the design objectives will have been met. The excellent

repeatability as shown in the first calibration tests insure that the absolute errors can be calibrated out. The sensitivities of the systems are such that the design requirement of a q range of 2 to 200 psf was easily met and surpassed. The pressure transducer sensing dynamic pressure by standard pitot tube techniques has an accuracy of better than 1 per cent. This insures a determination of velocity magnitude that is within the prescribed ± 1 per cent. It is difficult to test the probe fully without the use of a tunnel. Plans are to use the probe in Langley's new V-STOL wind tunnel when that facility becomes operational. The probe's full capabilities can best be examined at that time.

If a similar probe were to be constructed in the future, several recommendations should be offered. First, consideration should be given to the use of slip rings for the wires going to θ_2 servo components. With slip rings, motions of θ_1 need not be limited. Finally, an investigation could be made into the possibility of a more ideal orientation of the nulling ports on the probe face. Sensitivities could be improved, or cross coupled disturbances might be reduced.

In conclusion, it is felt that a useful instrument has been developed. While it is too large to be used in small wind tunnels, it should find application in many of the larger tunnels where subsonic investigations are made.

BIBLIOGRAPHY

1. Benedict, R. P. and W. E. Gunson. The Directional Pressure Probe - Cylindrical Type. Aviation Gas Turbine Division, Westinghouse Electric Corporation, Report No. A-1408, 1951.

2. Bryer, D. W., D. E. Walshe, and H. C. Garner. Pressure Probes Selected for Three-Dimensional Flow Measurement. Aerodynamics Division, National Physics Laboratory, R. & M. No. 3037. London: Her Majesty's Stationery Office, 1958.

3. Hundstad, Richard L. Three Dimensional Flow Measuring Probe. Midwestern Conference on Fluid Mechanics, Proceedings, 1952, pp. 521-529.

4. Richardson, Norman R. and Albin O. Pearson. Wind-Tunnel Calibrations of a Combined Pitot-Static Tube, Vane-Type Flow-Direction Transmitter, and Stagnation-Temperature Element at Mach Numbers From 0.60 to 2.87. NASA TN D-122, 1959.

5. Schulze, W. M., G. C. Ashby, Jr., and J. R. Erwin. Several Combination Probes for Surveying Static and Total Pressure and Flow Direction. NACA TN 2830, 1952.

6. Winternitz, F. A. L. "Probe Measurements in Three-Dimensional Flow," Aircraft Engineering, August 1956, pp. 273-278.

7. Krause, Lloyd N. and Thomas J. Dudginski. Flow-Direction Measurement With Fixed-Position Probes in Subsonic Flow Over a Range of Reynolds Numbers. ISA, National Aerospace Instrumentation Symposium, 15th, Las Vegas, Nevada, May 5-7, 1969.

8. Lee, J. C. and J. E. Ash. "A Three-Dimensional Spherical Pitot Probe," Transactions of the ASME, April 1956, pp. 603-607.

9. Norris, John D. Calibration of Conical Pressure Probes for Determination of Local Flow Conditions at Mach Numbers From 3 to 6. NASA TN D-3076, 1965.

10. Thomas, Robert N. A Flow Angularity Calibration of a 90° Cone Probe. Jet Propulsion Laboratory, California Institute of Technology, Technical Release No. 34-150, Pasadena, California, 1960.

11. Technical Description and Operating Instructions for NASA Flow-Direction and Pitot-Pressure Sensor. Nortronics Division, Northrup Corporation, NORT 60-46, 1960.

12. Shames, Irving H. Engineering Mechanics-Statics. Englewood Cliffs, New Jersey: Prentice-Hall, Inc., 1959.

13. _____. Engineering Mechanics-Dynamics. Englewood Cliffs, New Jersey: Prentice-Hall, Inc., 1960.

14. Sokolnikoff, I. S. and R. M. Redheffer. Mathematics of Physics and Modern Engineering, Second edition. New York: McGraw-Hill, 1966.

15. Savant, C. J., Jr. Control System Design. Second edition. New York: McGraw-Hill, 1964.

16. Newton, George C., Jr., Leonard A. Gould, and James F. Kaiser. Analytical Design of Linear Feedback Controls. Fourth printing, New York: John Wiley & Sons, Inc., 1967.

APPENDIX I

PRESSURE SENSITIVITY OF NULL SENSING PORTS

Tests were made in a model wind tunnel to determine the sensitivity of the null ports on the probe face. The probe was held fixed in a sting which could be accurately positioned in angle of attack. Port holes 1 and 2 were checked, and then the probe was rotated 90° for tests on holes 3 and 4. The sting was driven through offset angles (ϕ) of $\pm 4^{\circ}$. Figures II-1 and II-2 are plots of differential pressures between ports versus offset angles.

From these plots the sensitivity of both pairs of holes can be seen to be, 1×10^{-2} psi per degree offset. Since the tests were made at a q of 13.9×10^{-2} psi, the sensitivity can be expressed as:

$$\frac{P_{1-2}}{\Delta\phi_1} = \frac{P_{3-4}}{\Delta\phi_2} = (1 \times 10^{-2} \text{ psi/deg})\left(\frac{q}{13.9 \times 10^{-2} \text{ psi}}\right)$$

or

$$\frac{P_{1-2}}{\Delta\phi_1} = \frac{P_{3-4}}{\Delta\phi_2} = 0.07 \; q(\text{psi})/\text{deg}$$

Tests were run at other q values, and the hole sensitivity was always found to be 0.07 q(psi)/deg or 4 q(psi)/rad.

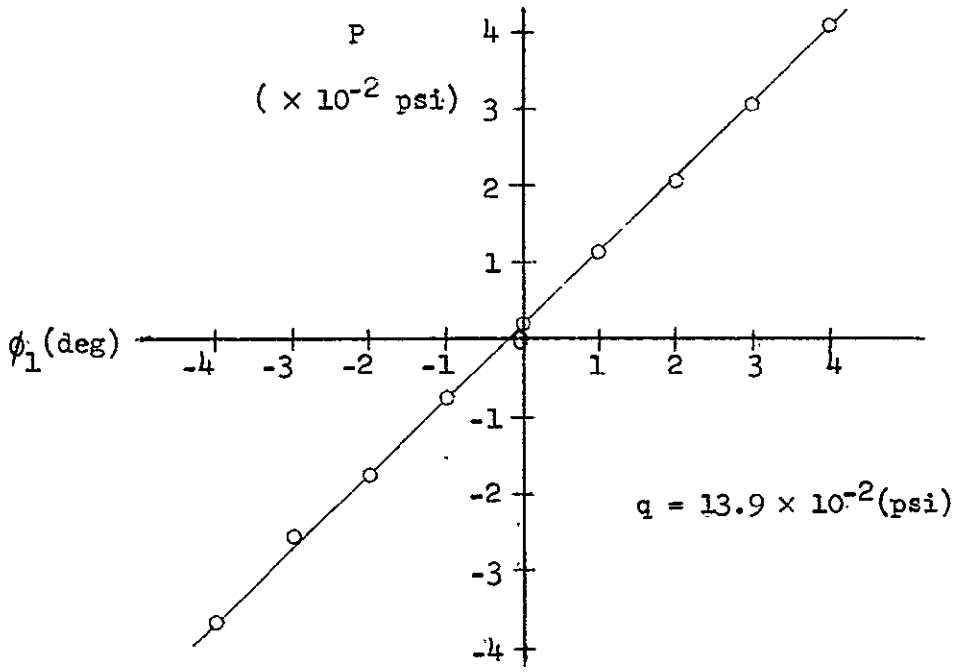

Figure I-1. Pressure sensitivity of ports 1-2.

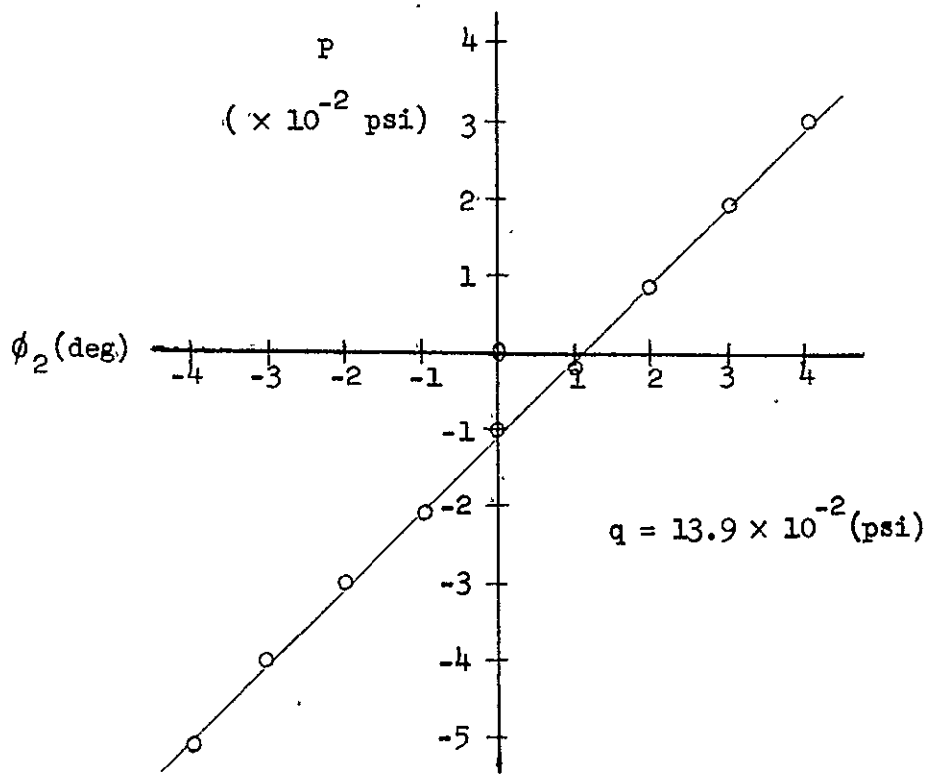

Figure I-2. Pressure sensitivity of ports 3-4.

APPENDIX II

DEVELOPMENT OF THE INNER LOOP TRANSFER FUNCTION

The speed-torque characteristics of a two-phase servomotor can be approximated by linear curves. A graphical representation of their relationship is shown in Figure II-1. The mathematical relationship is

$$L = - h\omega_m + b_o \tag{II-1}$$

Over a limited range the ratio of stall torque to applied voltage can also be considered linear. Figure II-2 illustrates this. From this curve

$$L_o = ke_a \tag{II-2}$$

is obtained. From Figure II-1 and equation (II-1) it can be seen that

$$b_o = L_o \tag{II-3}$$

and therefore,

$$L = - h\omega_m + ke_a \tag{II-4}$$

If the load is purely inertial

$$L = J \frac{d^2\theta_m}{dt^2} \tag{II-5}$$

and

$$J \frac{d^2\theta_m}{dt^2} = - h \frac{d\theta_m}{dt} + ke_a \tag{II-6}$$

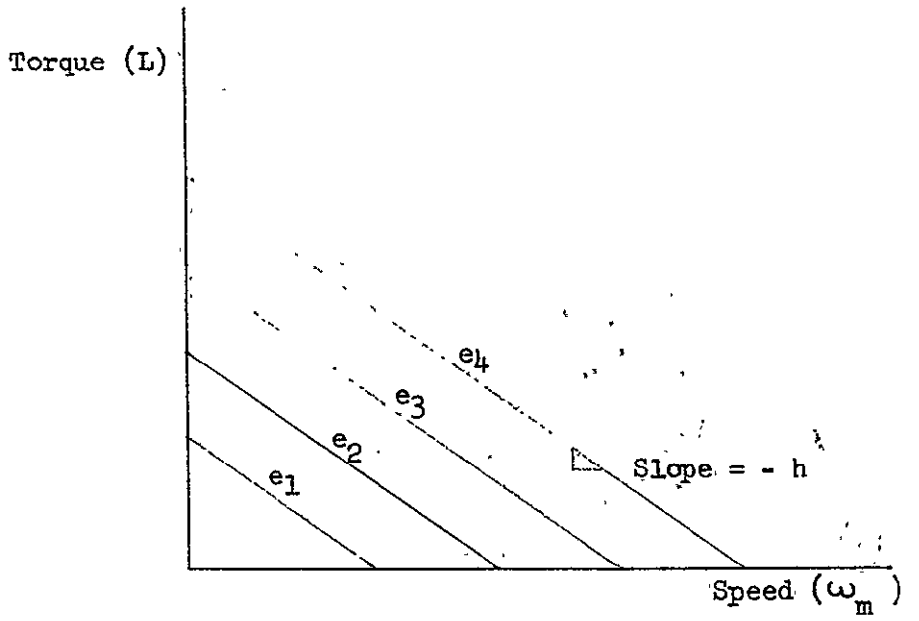

Figure II-1. Servomotor speed-torque curves.

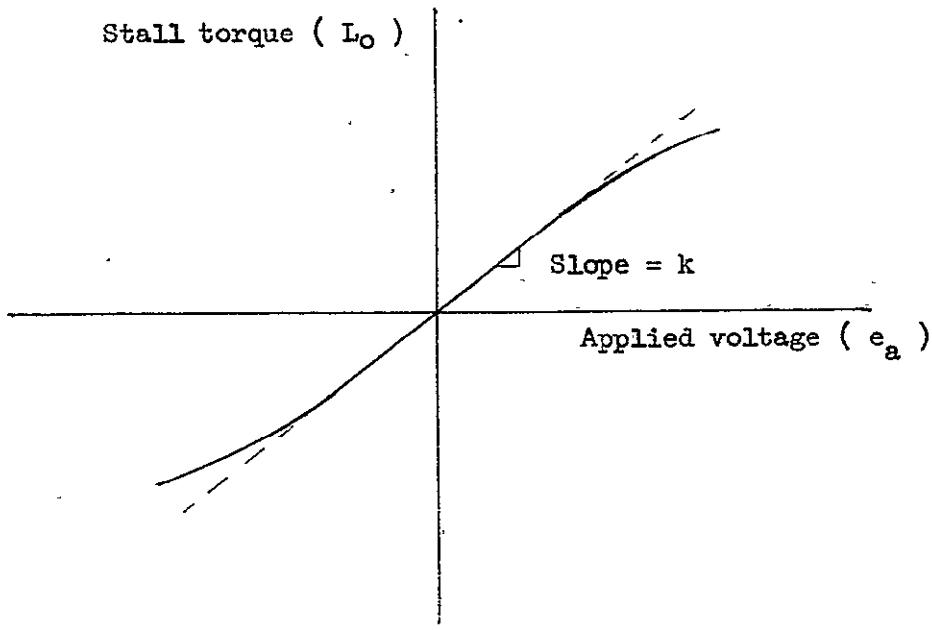

Figure II-2. Stall torque versus input voltage.

The LaPlace form of this equation is

$$JS^2\theta_m(S) = ke_a(S) - hS\theta_m(S) \qquad \text{(II-7)}$$

or

$$(JS^2 + hS)\theta_m(S) = ke_a(S) \qquad \text{(II-8)}$$

The transform of the motor can then be given as

$$\frac{\theta_m(S)}{e_a(S)} = \frac{k}{JS^2 + hS} \qquad \text{(II-9)}$$

Using the relations obtained from Figure 9 in the text,

$$e_a(S) = k_a e_\epsilon(S) \qquad \text{(II-10)}$$

$$e_\epsilon(S) = e_t(S) - e_g(S) \qquad \text{(II-11)}$$

and,

$$e_g(S) = k_g S\theta_m(S) \qquad \text{(II-12)}$$

The inner loop transfer function is

$$G'(S) = \frac{\theta_m(S)}{e_t(S)} = \frac{\frac{kk_a}{J}}{S\left(S + \frac{h + kk_a k_g}{J}\right)} \qquad \text{(II-13)}$$

APPENDIX III

ROOT LOCUS PLOTS AND SYSTEM CONSTANTS

The open loop transfer function, K_V and τ were described in the text (equations 77-79) as,

$$G(S)H(S) = G(S) = \frac{\frac{K_V\gamma}{\tau}}{S\left(S + \frac{1}{\tau}\right)(S + \gamma)} \qquad \text{(III-1)}$$

and

$$K_V = \frac{K_T}{\left(\frac{h + kk_ak_g}{J}\right)\gamma} \qquad \text{(III-2)}$$

where

$$K_T = \frac{k_vk_pk_tkk_ak_n\gamma}{J} \qquad \text{(III-3)}$$

and

$$\tau = \frac{J}{h + kk_ak_g} \qquad \text{(III-4)}$$

The closed loop transfer function given in the canonical form is

$$\frac{C}{R} = \frac{G}{1 + GH} = \frac{\frac{K_V\gamma}{\tau}}{S^3 + \left(\gamma + \frac{1}{\tau}\right)S^2 + \frac{\gamma}{\tau}S + \frac{K_V\gamma}{\tau}} \qquad \text{(III-5)}$$

The characteristic equation is

$$S^3 + \left(\gamma + \frac{1}{\tau}\right)S^2 + \frac{\gamma}{\tau}S + \frac{K_V\gamma}{\tau} = 0 \qquad \text{(III-6)}$$

2

The closed loop poles are then found from the following constants:

θ_1 System

The θ_1 system constants are:

$$k_{v_1} = 0.384 \sin \theta_2'$$

$$k_{p_1} = 4\ q \text{ psi/rad}$$

$$k^*_{t_1} = 5/q \quad \text{volt/psi (minimum transducer gain for probe threshold at } \phi_1 = 0.5^\circ)$$

$$k_1 = 10^{-2} \text{ oz-in/volt}$$

$$k^*_{a_1} = 64$$

$$k_{n_1} = 5.04 \times 10^{-4}$$

$$J_1 = 8.35 \times 10^{-6} \text{ oz-in-sec}^2/\text{rad}$$

$$K_{T_1} = 1.47 \times 10^4 \sin \theta_2' \text{ sec}^{-3}$$

$$h_1 = 4.0 \times 10^{-4} \text{ oz-in-sec /rad}$$

$$k^*_{g_1} = 3 \times 10^{-3} \text{ volt-sec/rad}$$

$$K_{V_1} = 1.06 \sin \theta_2' \text{ sec}^{-1}$$

$$\tau_1 = 3.6 \times 10^{-3} \text{ sec}$$

$$\gamma_1 = 50 \text{ sec}^{-1}$$

*These constants are adjustable.

The open loop poles are

$$S = 0, \quad S = -50, \text{ and } S = -278$$

The closed loop poles are

$S = 0, -50$, and -278 $\quad (\theta_2' = 0)$

$S = -1.1, -48.7$, and -278.7 $\quad (\theta_2' = 90^\circ)$

The root locus plot for the θ_1 system with $\theta_2' = 90^\circ$ is shown in Figure III-1. As θ_2 approaches 0° or 180° from 90° the closed loop poles approach the open loop poles.

θ_2 System

The θ_2 system constants are:

$$k_{v_2} = 0.384$$

$$k_{p_2} = 4 \text{ q psi/rad}$$

$$k^*_{t_2} = 5/q \text{ volt/psi} \quad \text{(minimum transducer gain for probe threshold at } \phi_2 = 0.5^\circ)$$

$$k_2 = 10^{-2} \text{ oz-in/volt}$$

$$k^*_{a_2} = 25$$

$$k_{n_2} = 6.91 \times 10^{-4}$$

$$J_2 = 8.35 \times 10^{-6} \text{ oz-in-sec/rad}$$

$$K_{T_2} = 7.9 \times 10^{3} \text{ sec}^{-3}$$

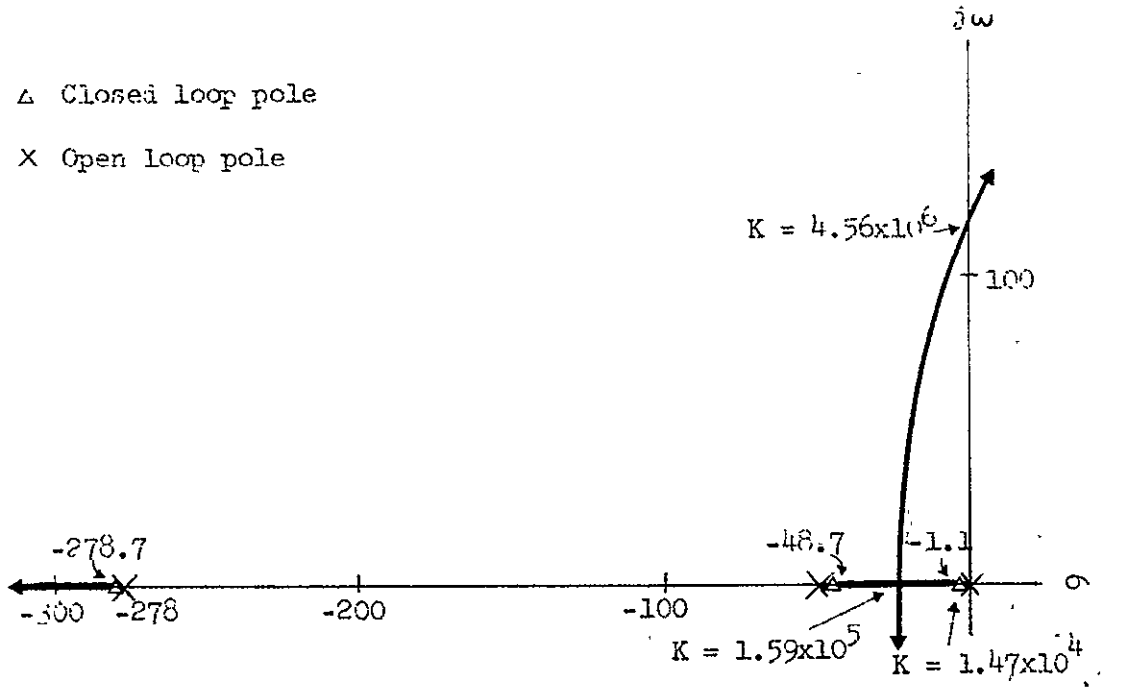

Figure III-1. Root locus for θ_1 system ($\theta_2' = 90°$).

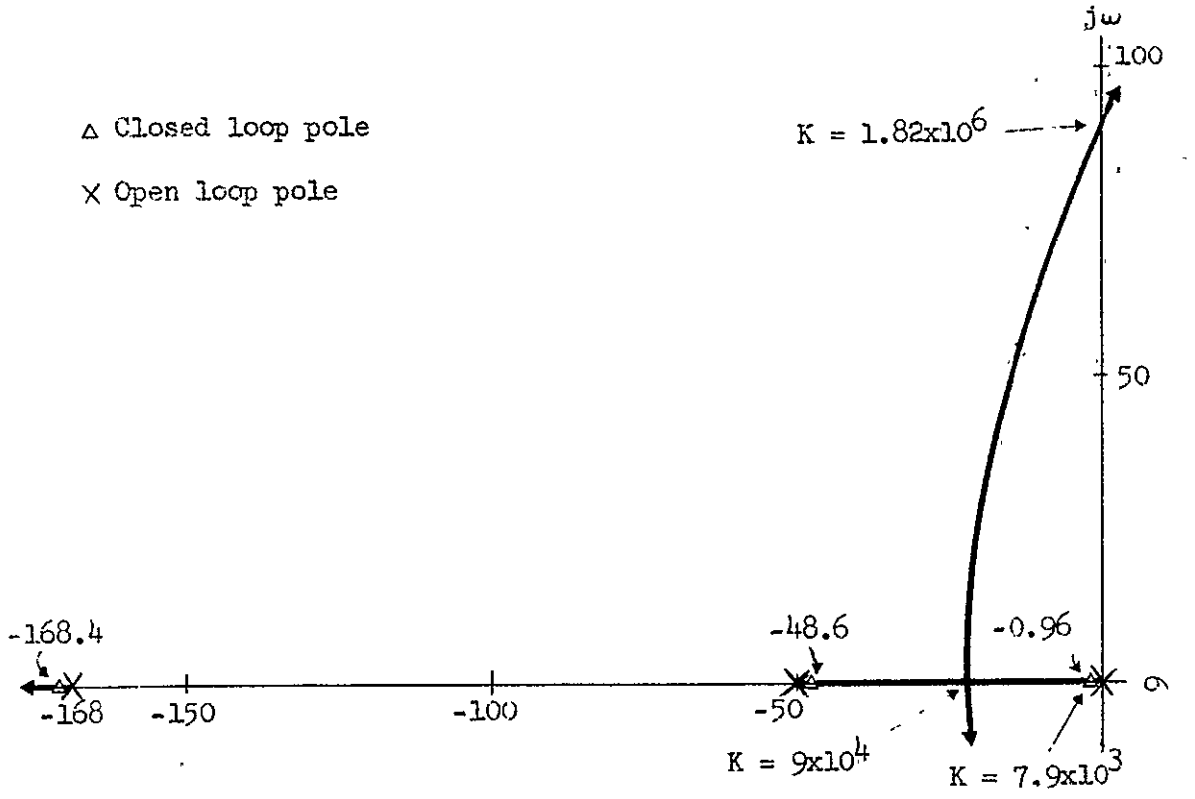

Figure III-2. Root locus for θ_2 system.

$$h_2 = 4.0 \times 10^{-4} \text{ oz-in-sec/rad}$$

$$k^*_{g_2} = 4 \times 10^{-3} \text{ volt-sec/rad}$$

$$K_{V_2} = 0.94 \text{ sec}^{-1}$$

$$\tau_2 = 5.96 \times 10^{-3} \text{ sec}$$

$$\gamma_2 = 50 \text{ sec}^{-1}$$

*These constants are adjustable.

The open loop poles are

$$S = 0, -50, \text{ and } -168$$

The closed loop poles are

$$S = -0.96, -48.6, \text{ and } -168.4$$

The root locus plot for the θ_2 system is shown in Figure III-2.

PRECEDING PAGE BLANK NOT FILMED.

FOLDOUT FRAME 1

FOLDOUT FRAME 2

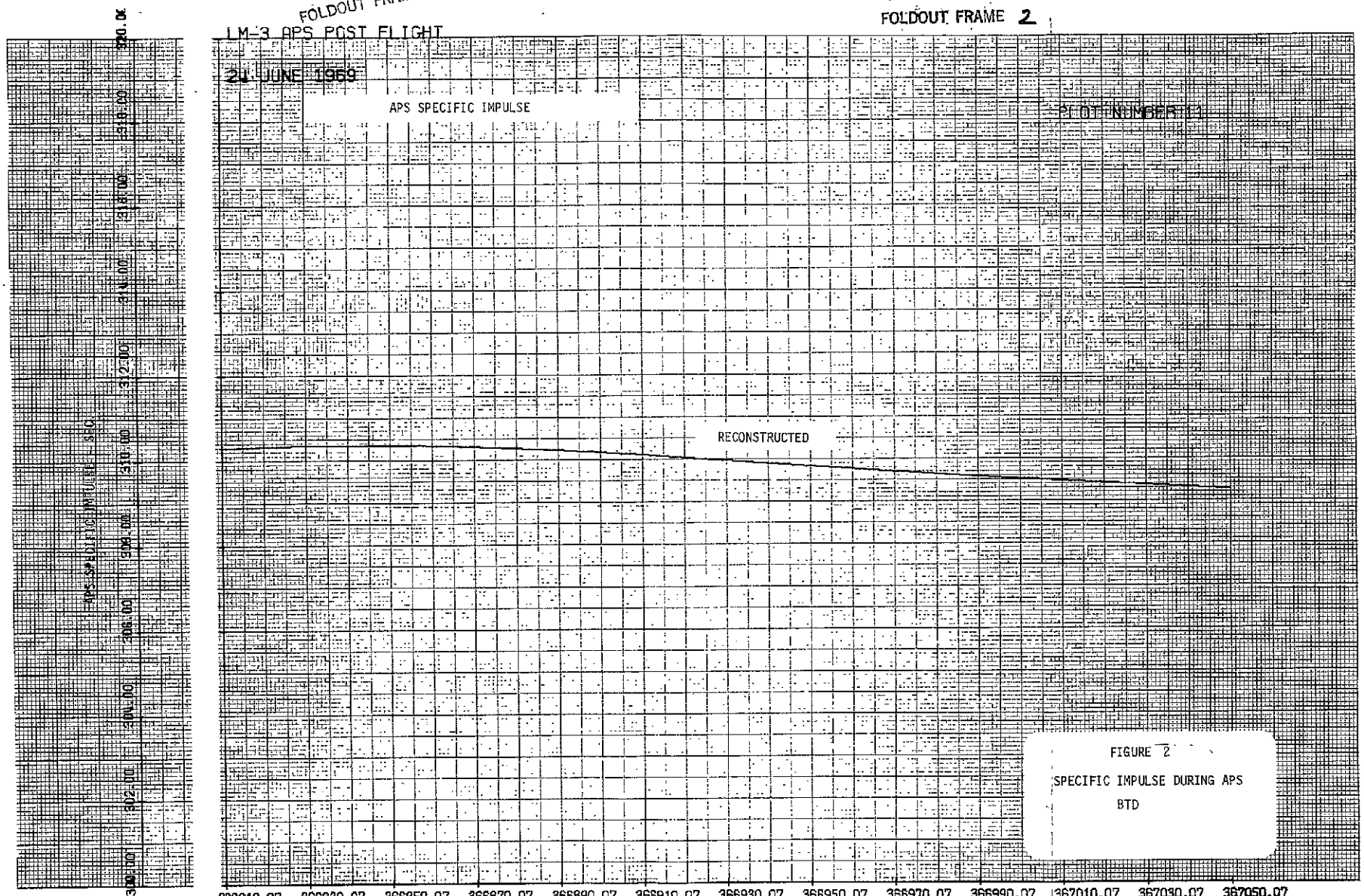

FIGURE 2

SPECIFIC IMPULSE DURING APS

BTD

FOLDOUT FRAME

FIGURE 3

THROAT AREA VS. SPECIFIC IMPULSE

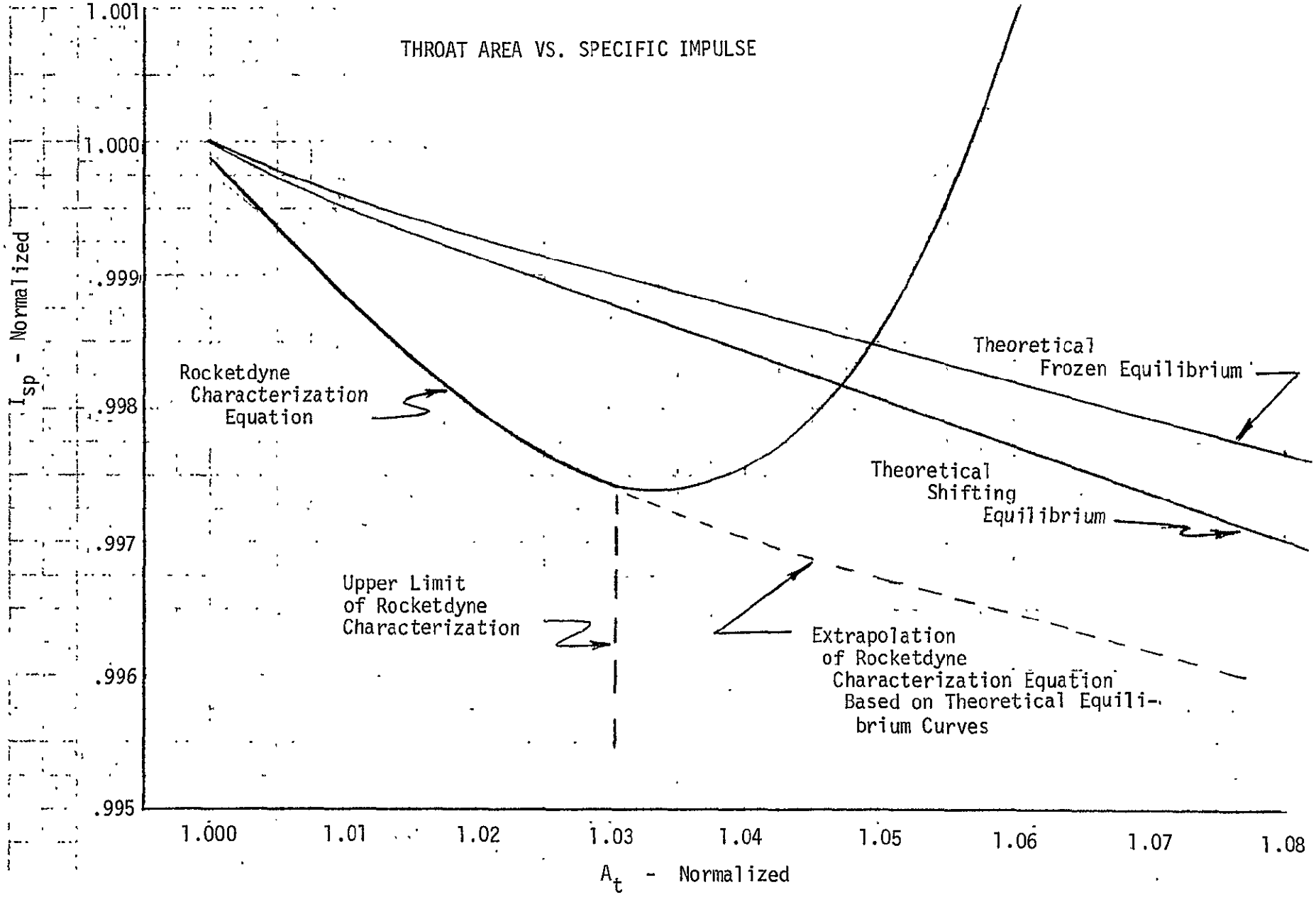

FOLDOUT FRAME

FIGURE 4.

COMPARISON OF PRESSURE TRENDS, FLIGHT AND RECONSTRUCTION VS. REPREDICTED

FOLDOUT FRAME 2

FOLDOUT FRAME 2

FOLDOUT FRAME 1

FOLDOUT FRAME 2

FOLDOUT FRAME 2

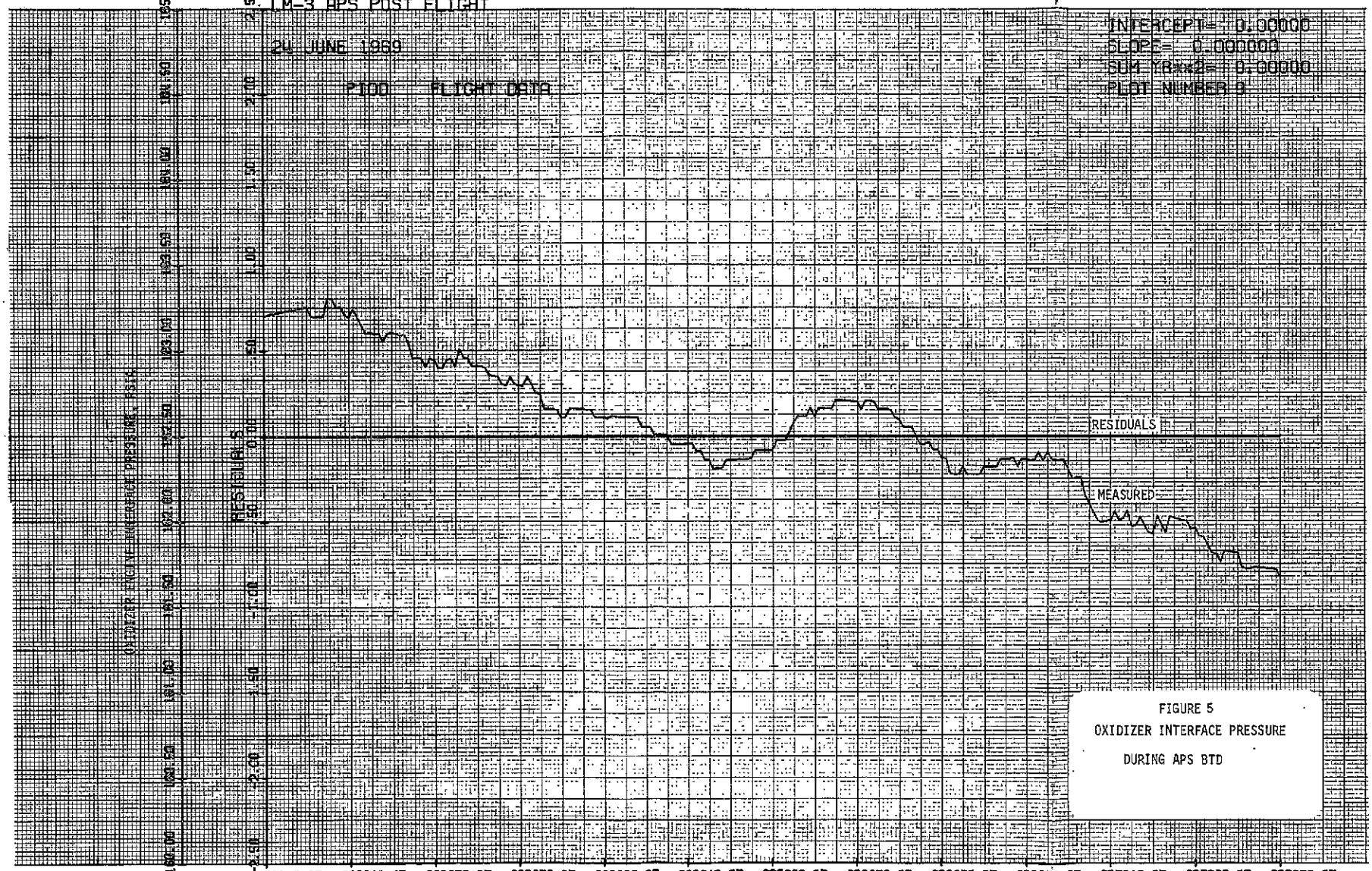

FIGURE 5
OXIDIZER INTERFACE PRESSURE
DURING APS BTD

FOLDOUT FRAME 1

FOLDOUT FRAME 2

FOLDOUT FRAME 2

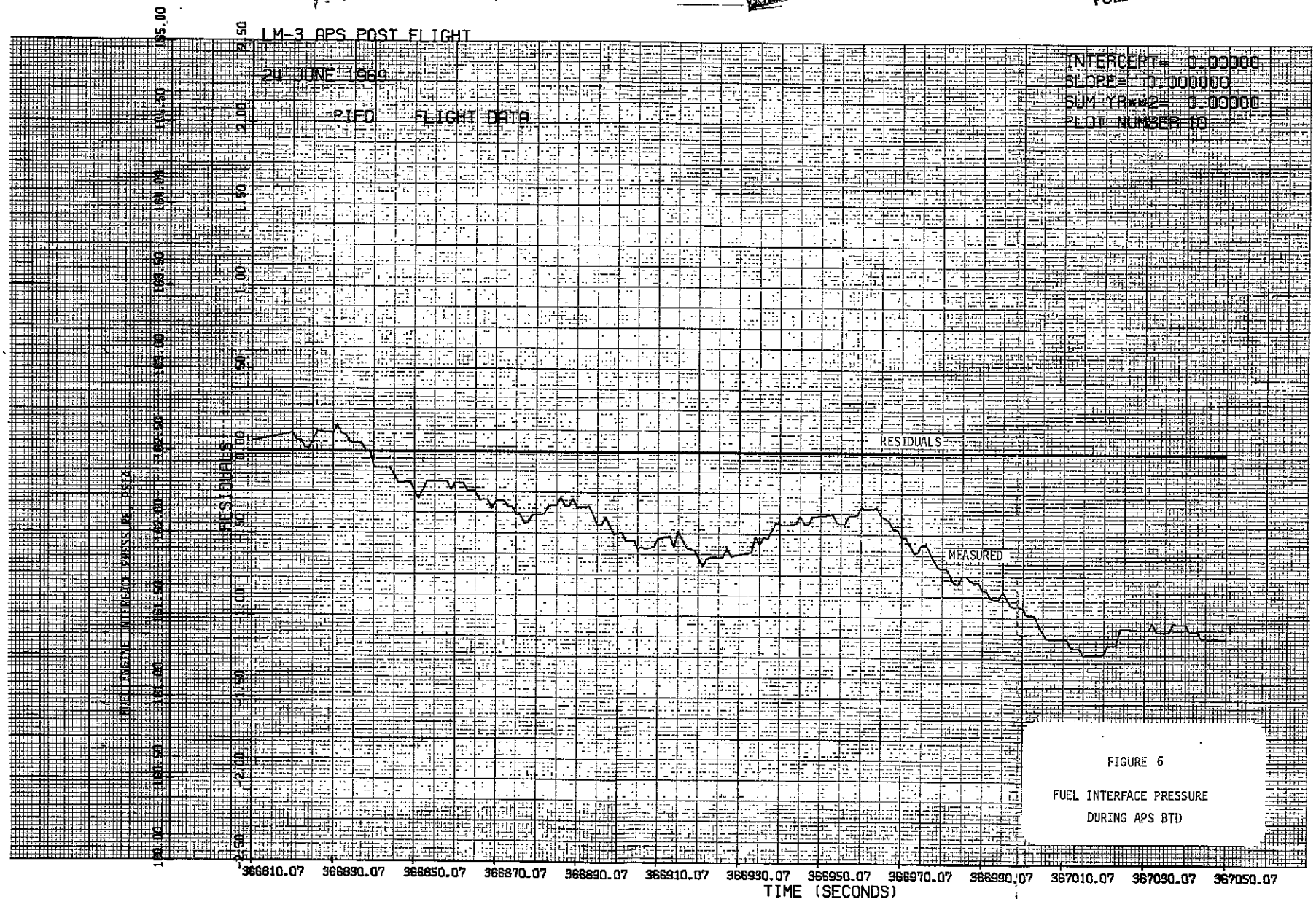

FIGURE 6

FUEL INTERFACE PRESSURE
DURING APS BTD

FOLDOUT FRAME 1

FOLDOUT FRAME 2

FOLDOUT FRAME 2

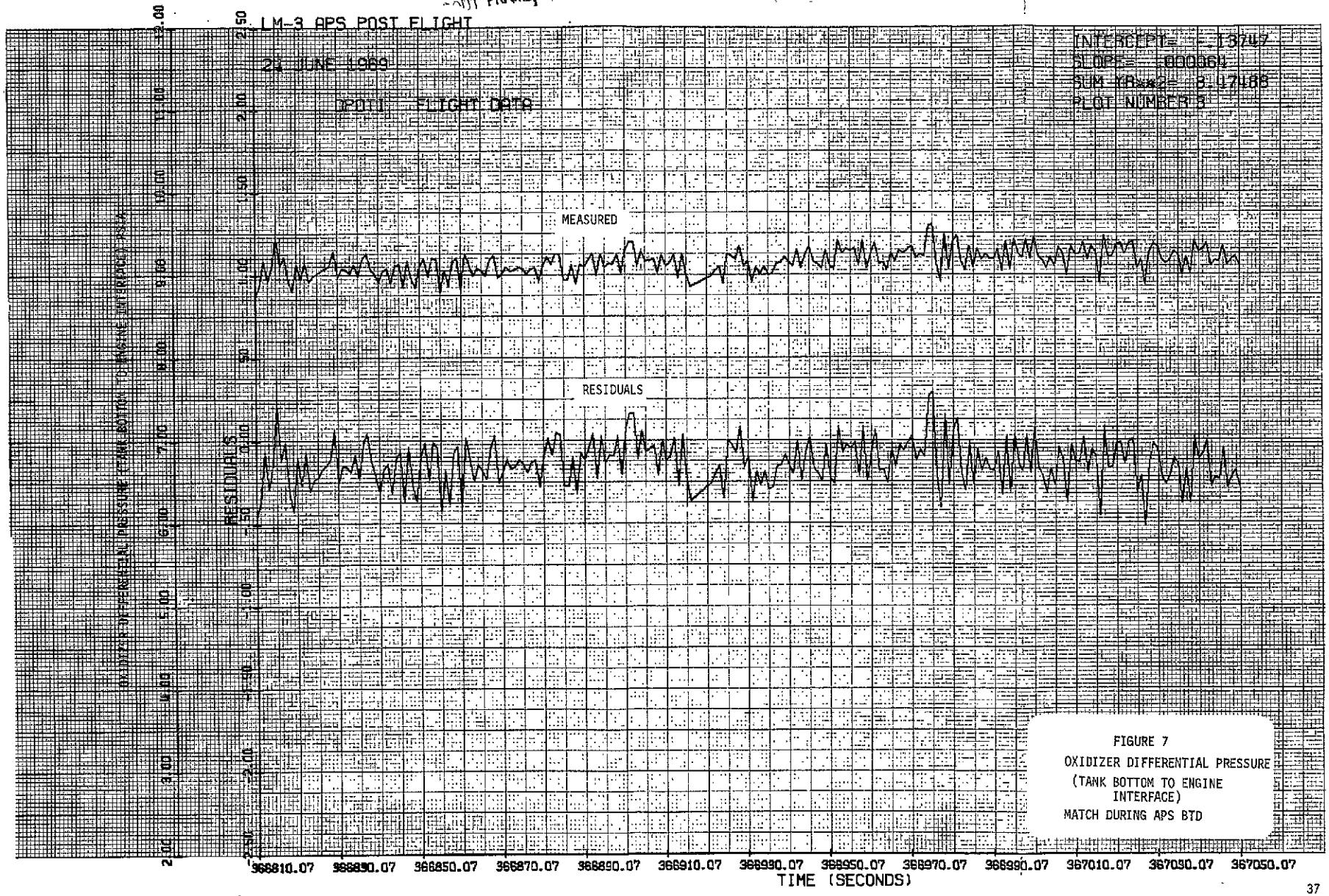

FIGURE 7
OXIDIZER DIFFERENTIAL PRESSURE
(TANK BOTTOM TO ENGINE INTERFACE)
MATCH DURING APS BTD

FOLDOUT FRAME 1

FOLDOUT FRAME 2

FOLDOUT FRAME 2

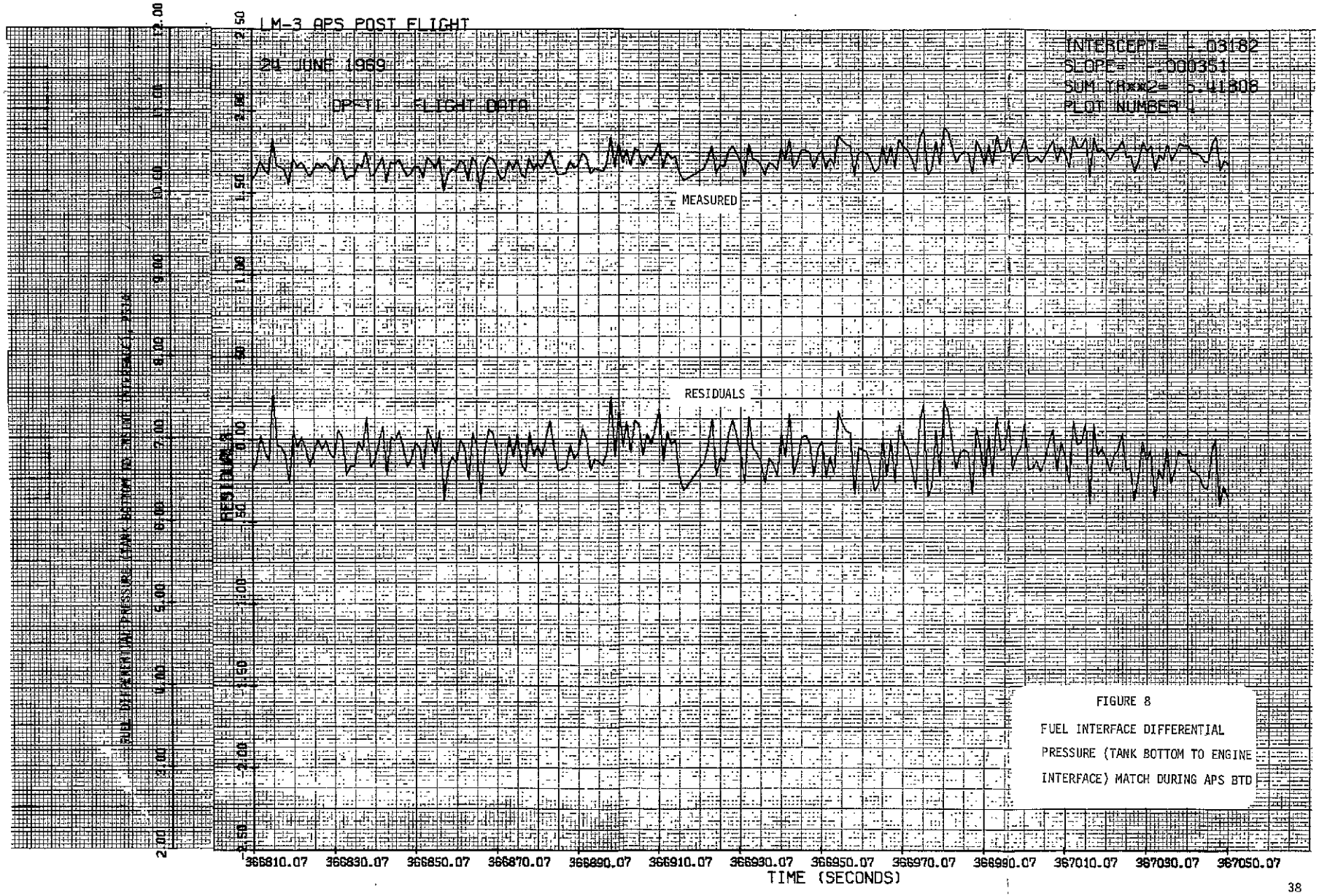

FIGURE 8

FUEL INTERFACE DIFFERENTIAL PRESSURE (TANK BOTTOM TO ENGINE INTERFACE) MATCH DURING APS BTD

FOLDOUT FRAME 1

FOLDOUT FRAME 2

FOLDOUT FRAME 2

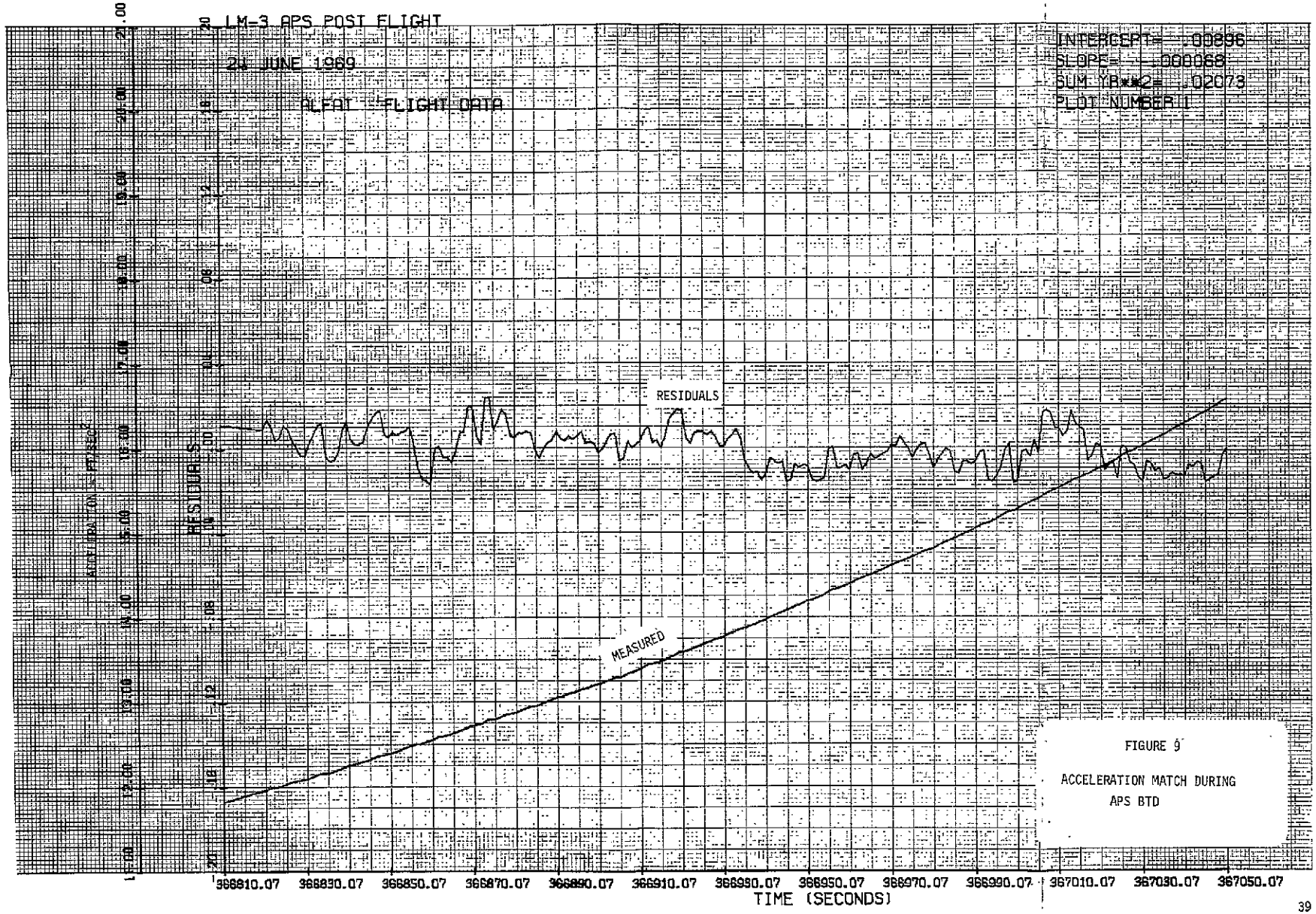

FIGURE 9

ACCELERATION MATCH DURING APS BTD

FOLDOUT FRAME 1

FOLDOUT FRAME 2

FOLDOUT FRAME 2

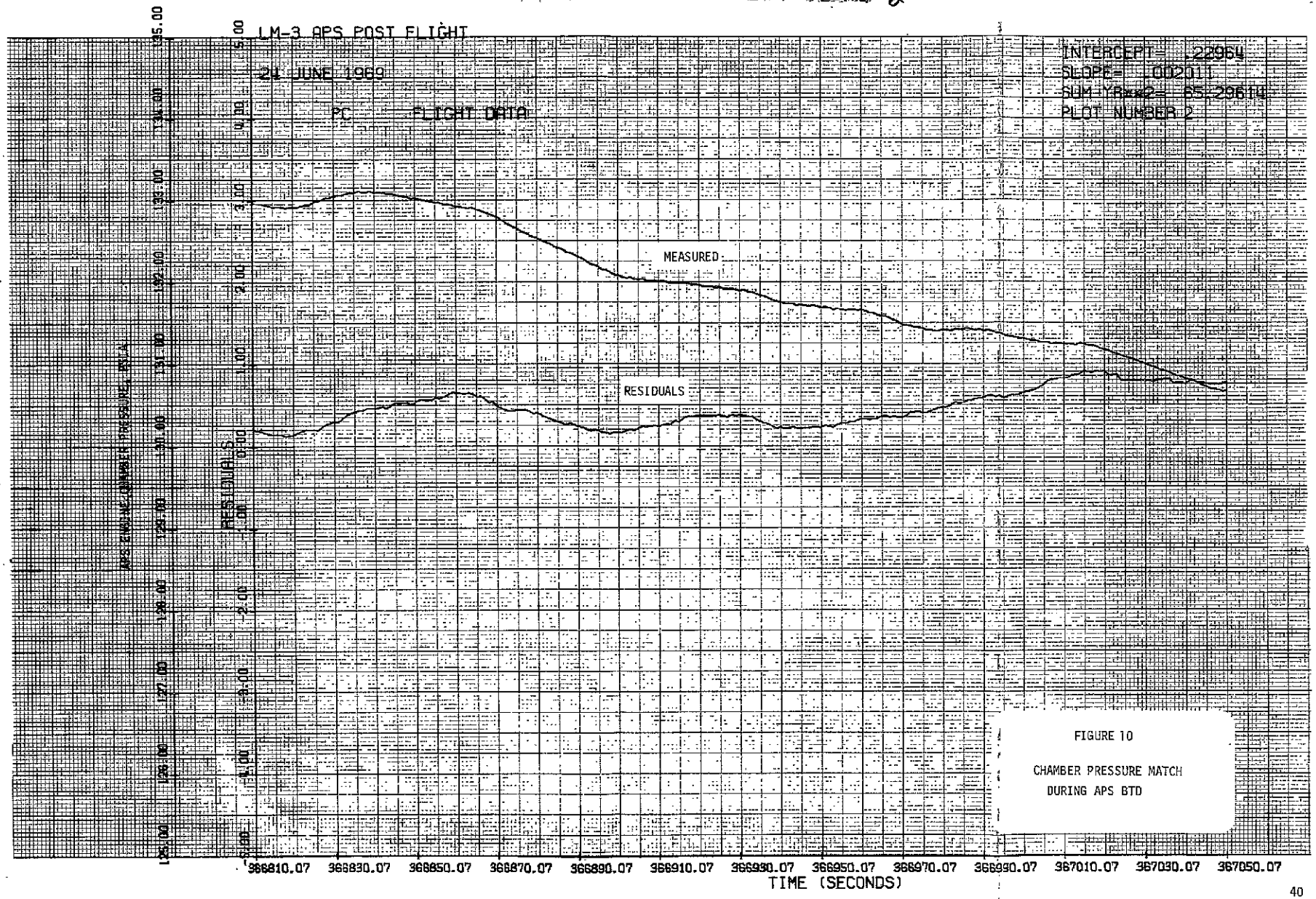

FIGURE 10

CHAMBER PRESSURE MATCH
DURING APS BTD

FOLDOUT FRAME 1

FOLDOUT FRAME 2

FOLDOUT FRAME 2

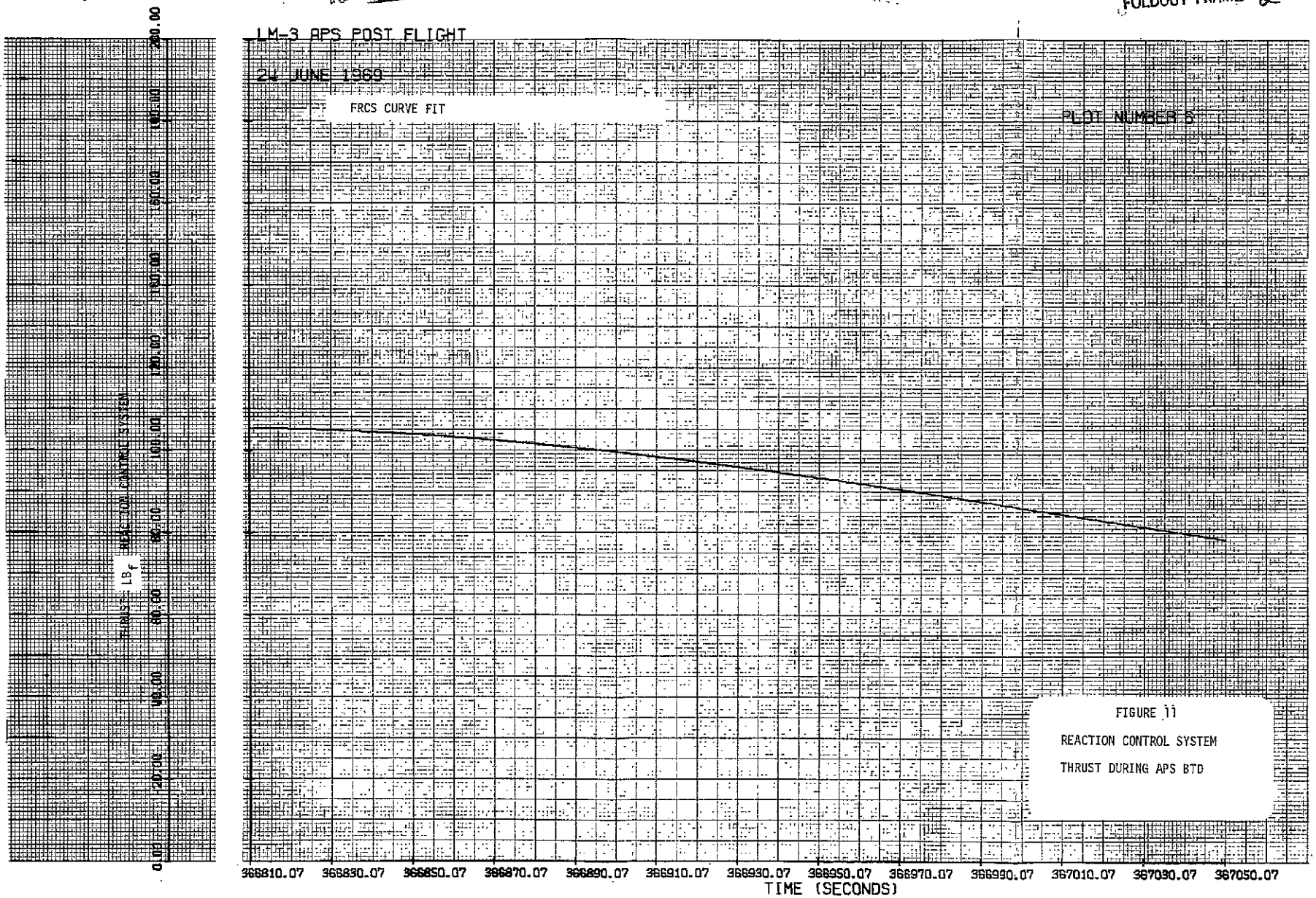

FIGURE 11

REACTION CONTROL SYSTEM

THRUST DURING APS BTD

FOLDOUT FRAME 1

FOLDOUT FRAME 2

FOLDOUT FRAME 2

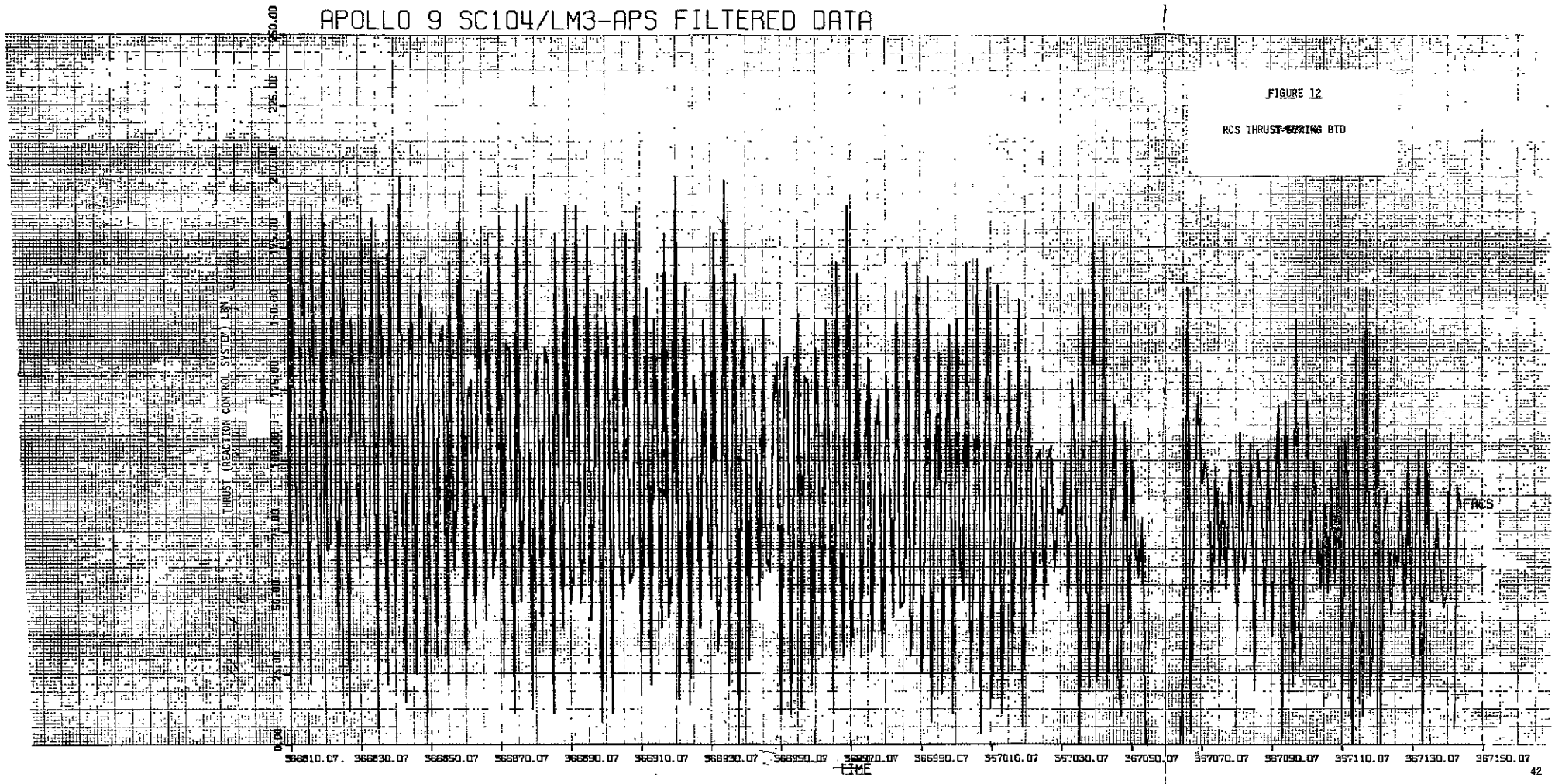

FOLDOUT FRAME 1

FOLDOUT FRAME 2

FOLDOUT FRAME 2

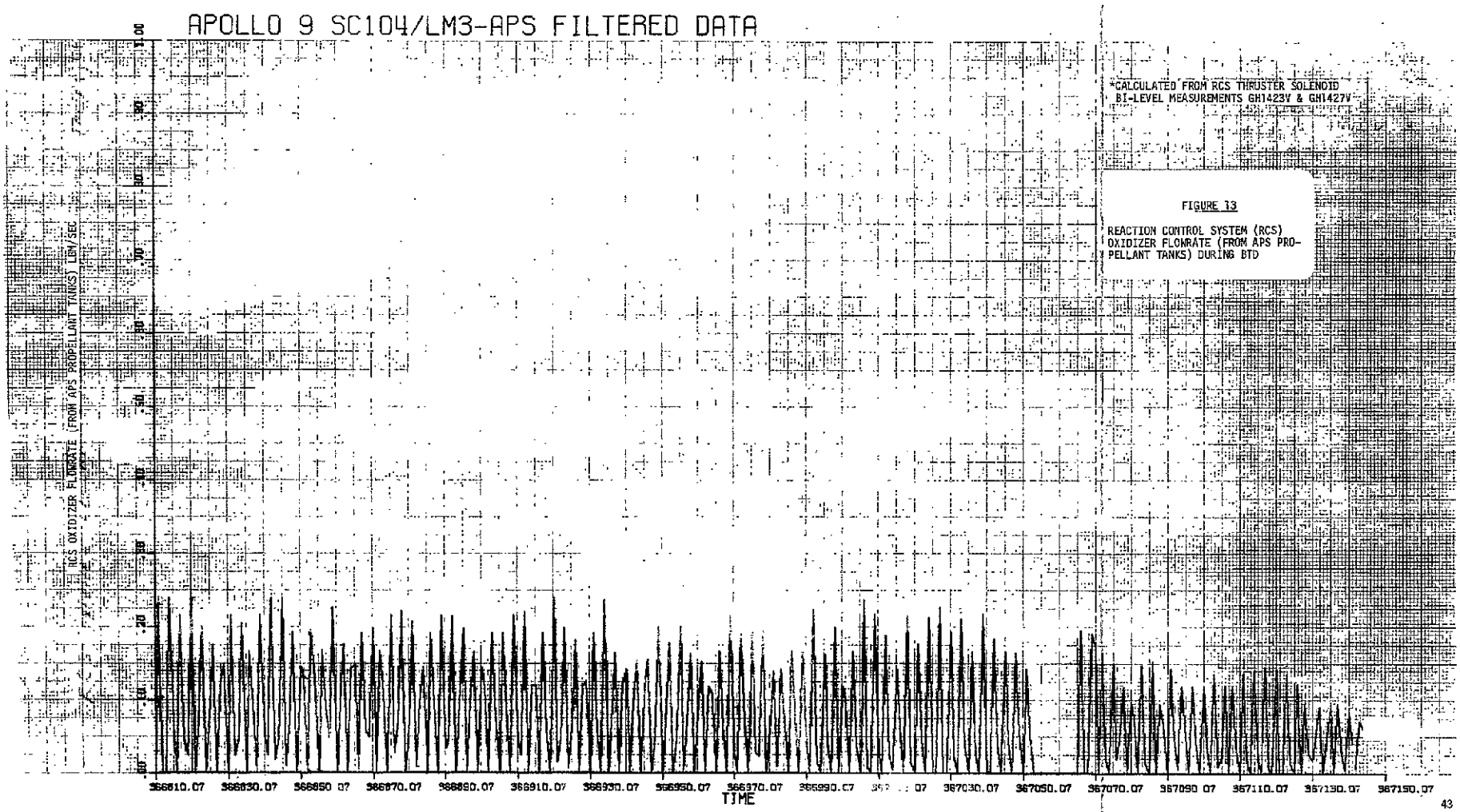

FIGURE 13

REACTION CONTROL SYSTEM (RCS) OXIDIZER FLOWRATE (FROM APS PROPELLANT TANKS) DURING BTD

FOLDOUT FRAME 1

FOLDOUT FRAME 2

FOLDOUT FRAME 2

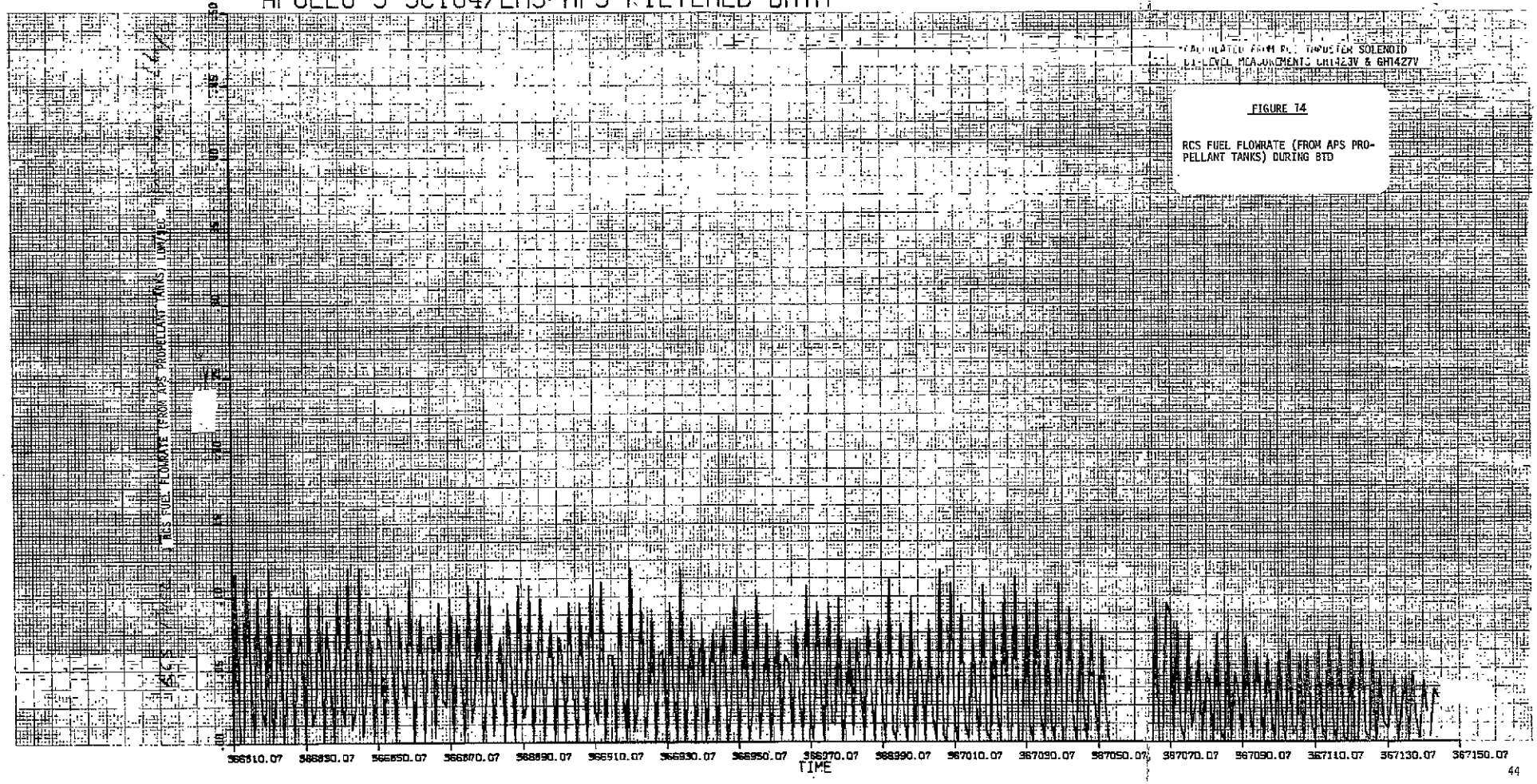

FOLDOUT FRAME 1

FOLDOUT FRAME 2

FOLDOUT FRAME 2

APOLLO 9 SC104/LM3-APS FILTERED DATA

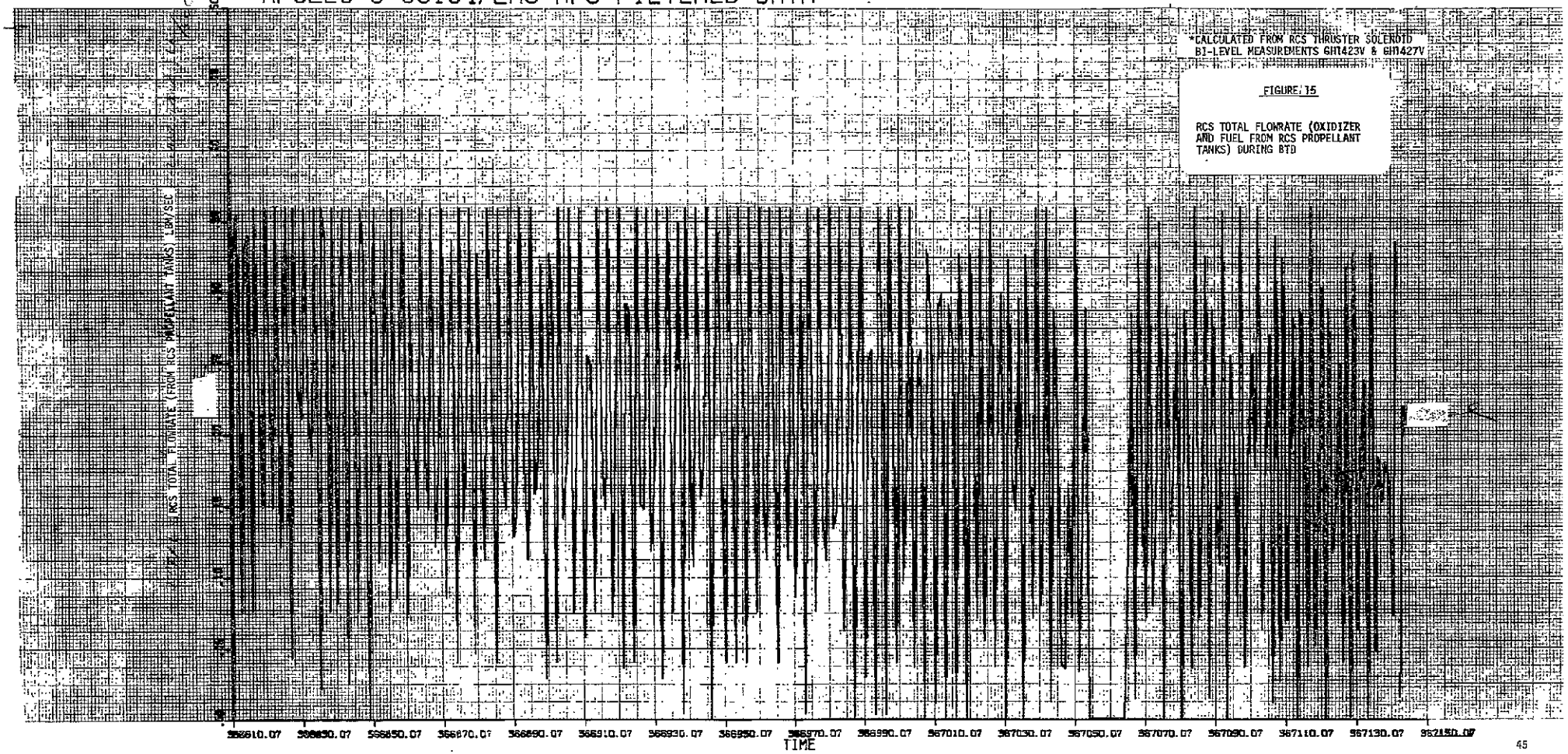

FIGURE 15

RCS TOTAL FLOWRATE (OXIDIZER AND FUEL FROM RCS PROPELLANT TANKS) DURING BTD

FOLDOUT FRAME 1

FOLDOUT FRAME 2

FOLDOUT FRAME 2

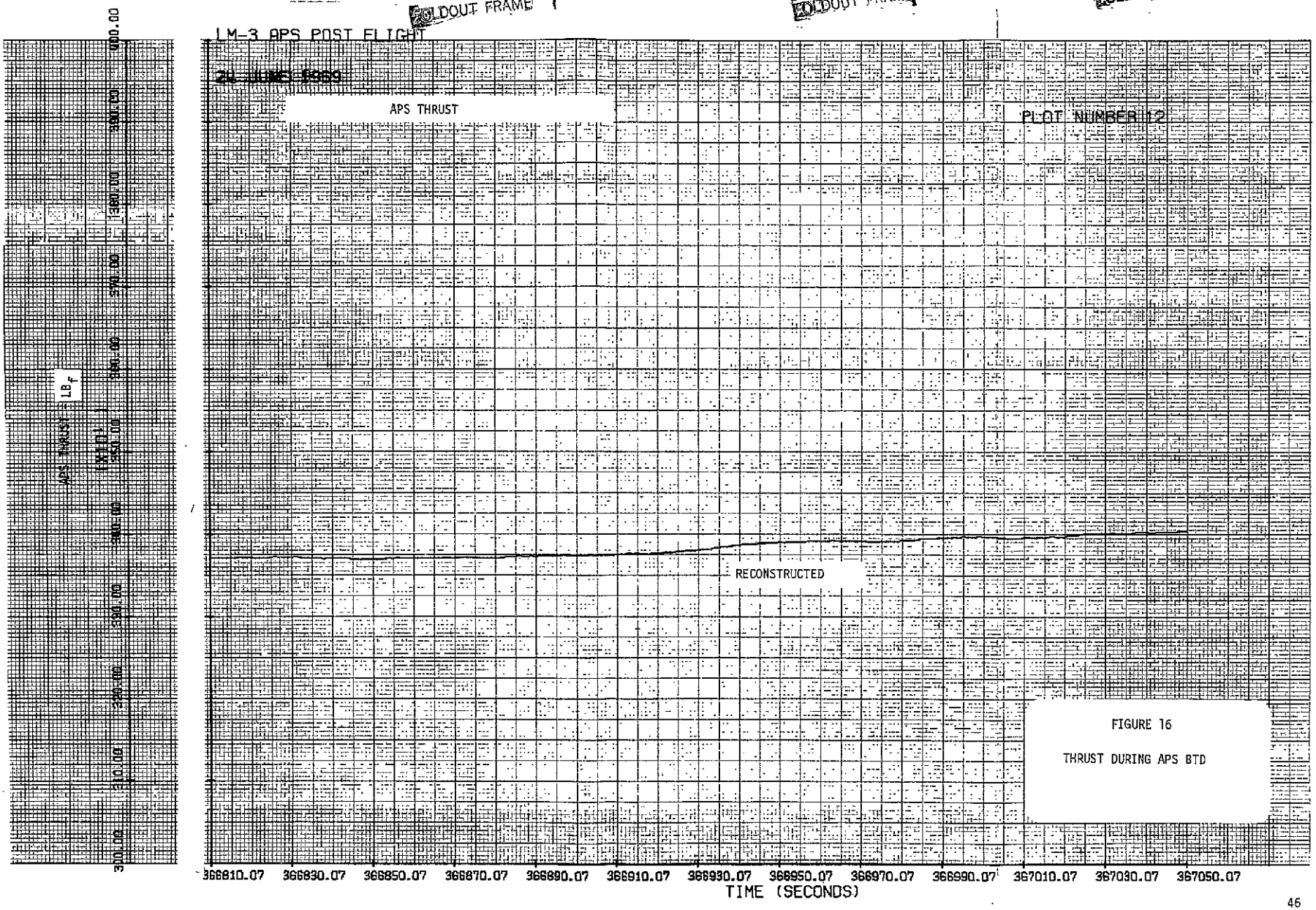

FIGURE 16

THRUST DURING APS BTD

FOLDOUT FRAME 1

FOLDOUT FRAME 2

FOLDOUT FRAME 2

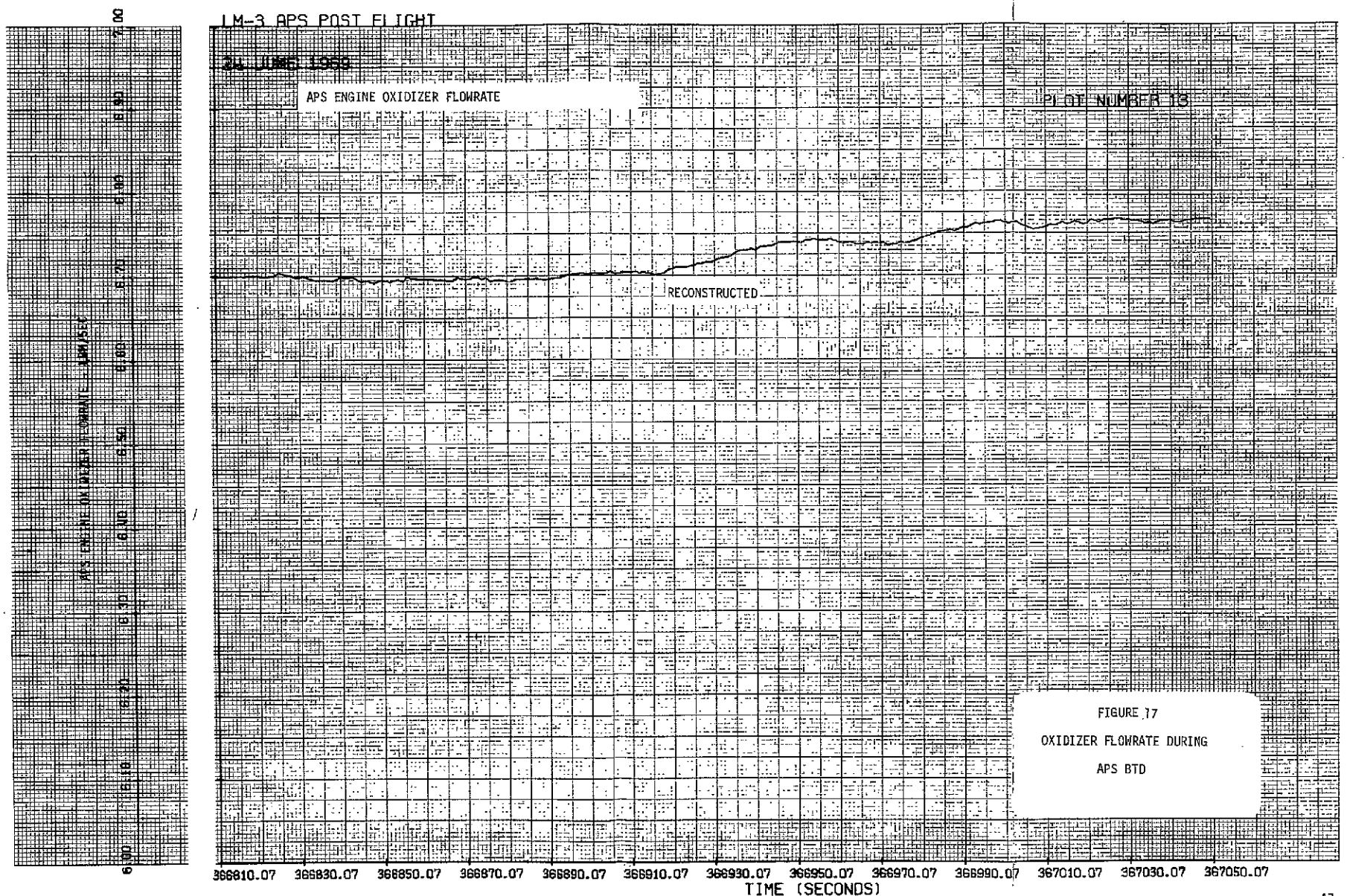

FIGURE 17

OXIDIZER FLOWRATE DURING

APS BTD

FOLDOUT FRAME 1

FOLDOUT FRAME 2

FOLDOUT FRAME 2

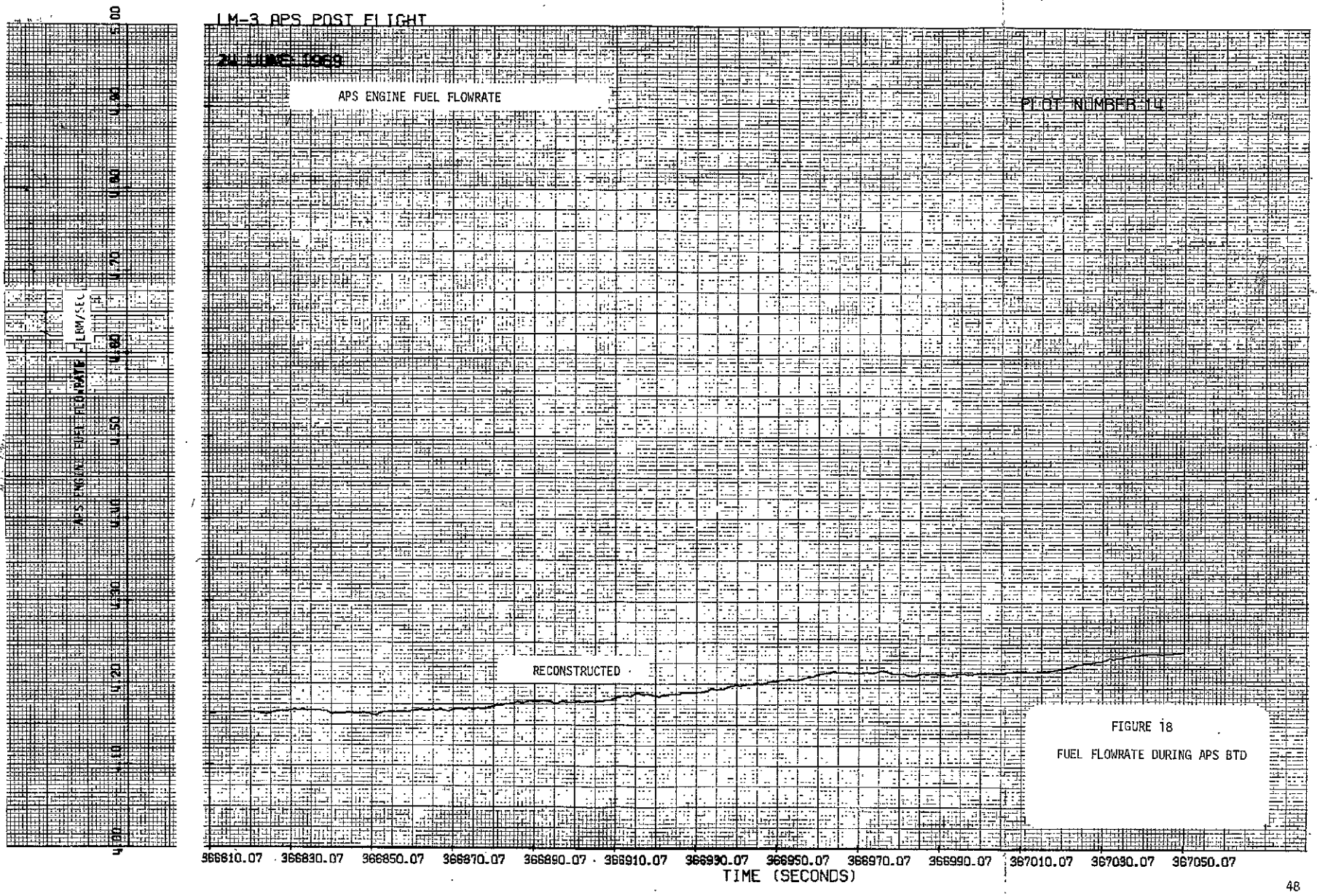

FIGURE 18

FUEL FLOWRATE DURING APS BTD

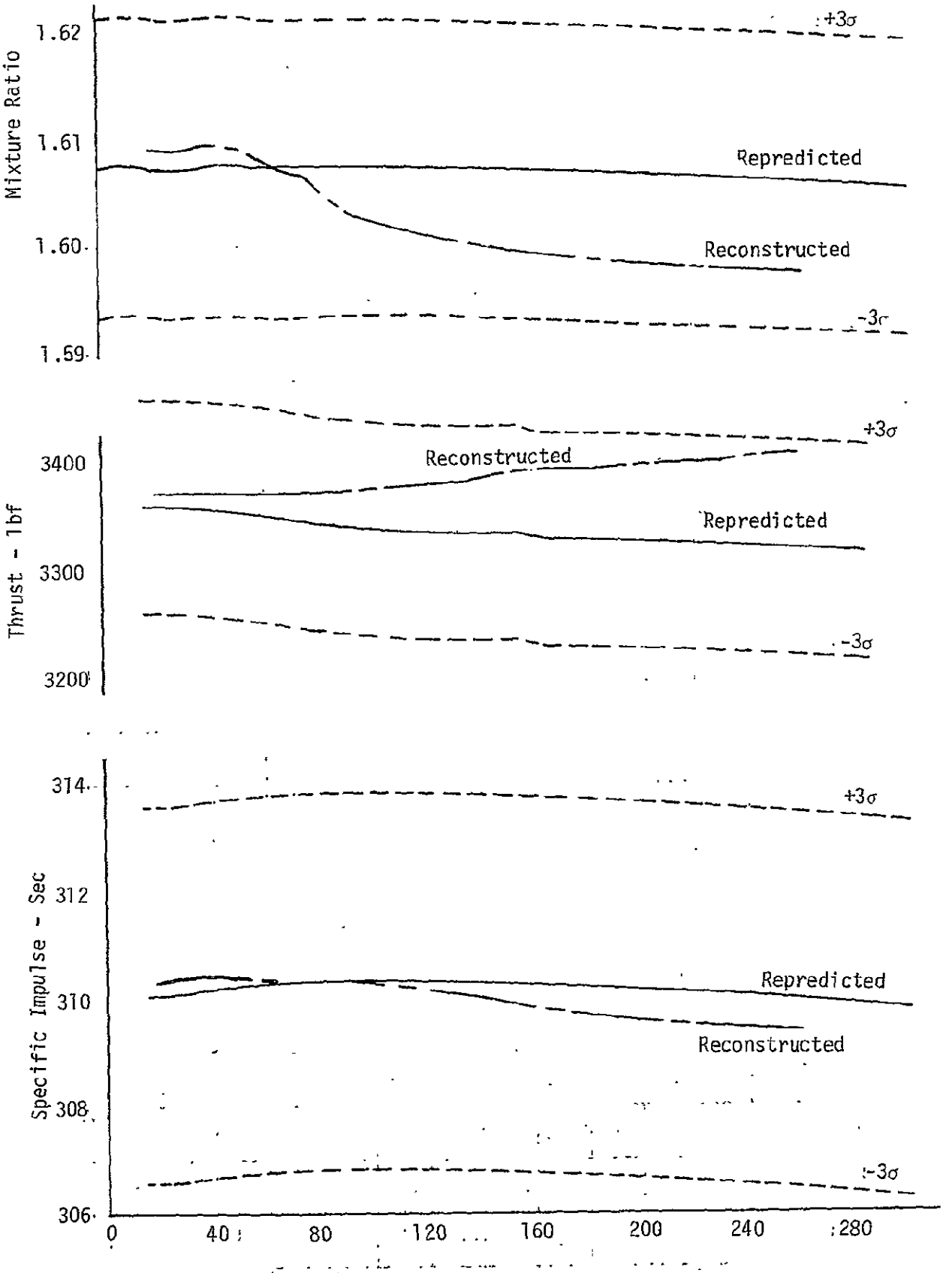

Figure 19 Comparison of Repredicted and Flight Reconstructed Performance

FIGURE 20

HELIUM SUPPLY TANKS PRESSURE

DURING BTD

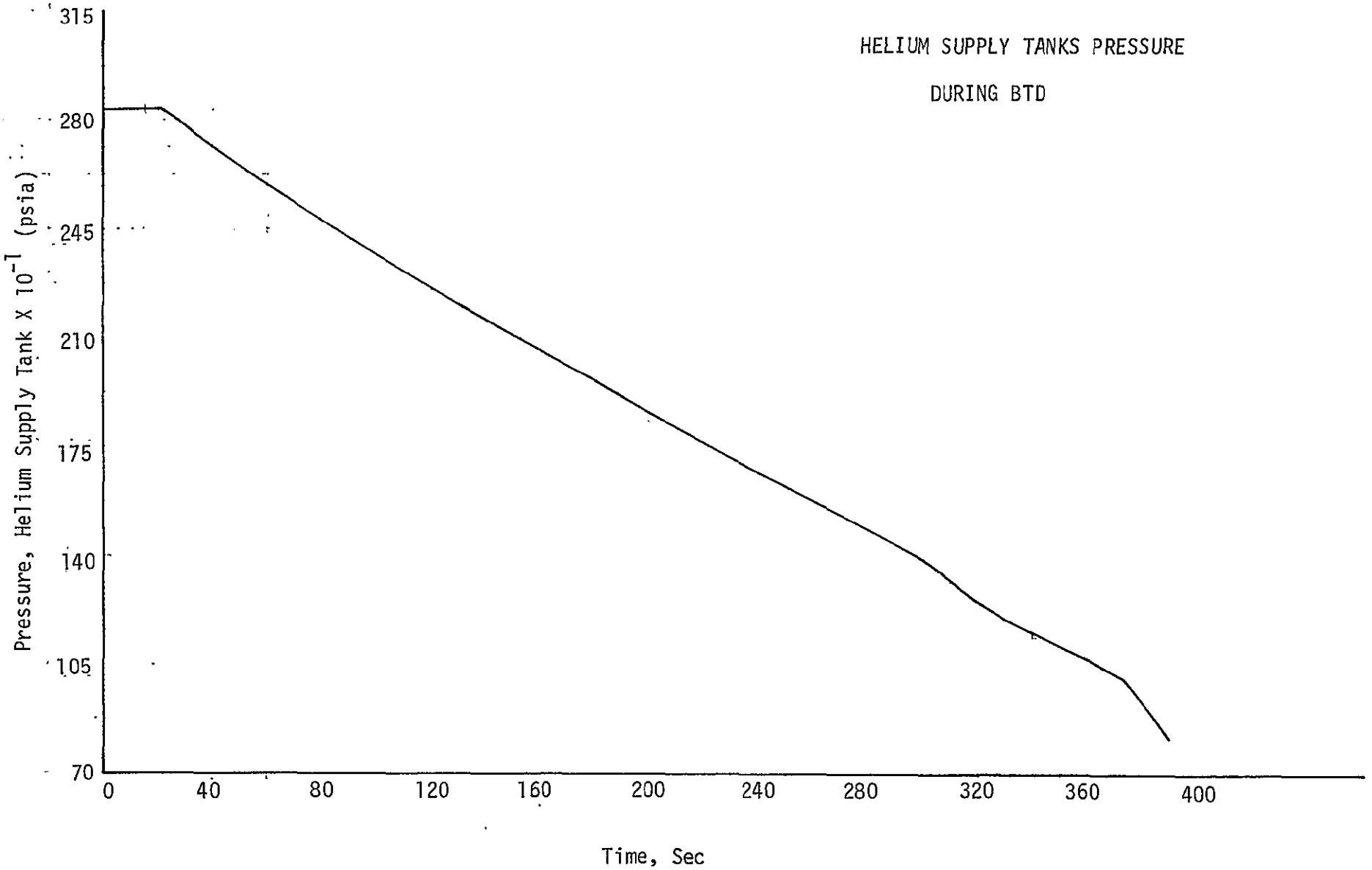

FIGURE 21

REGULATOR OUT PRESSURE DURING

BTD

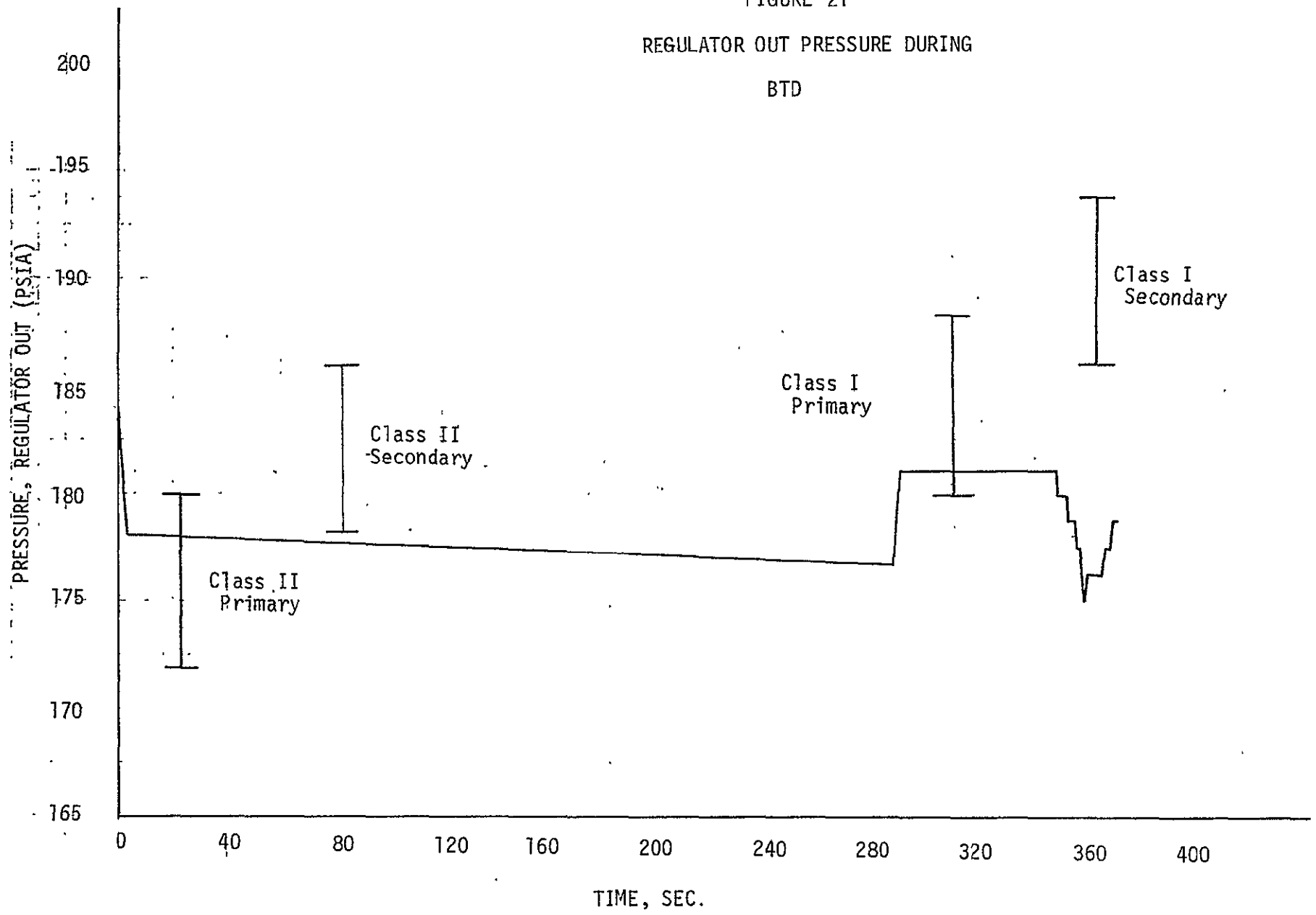

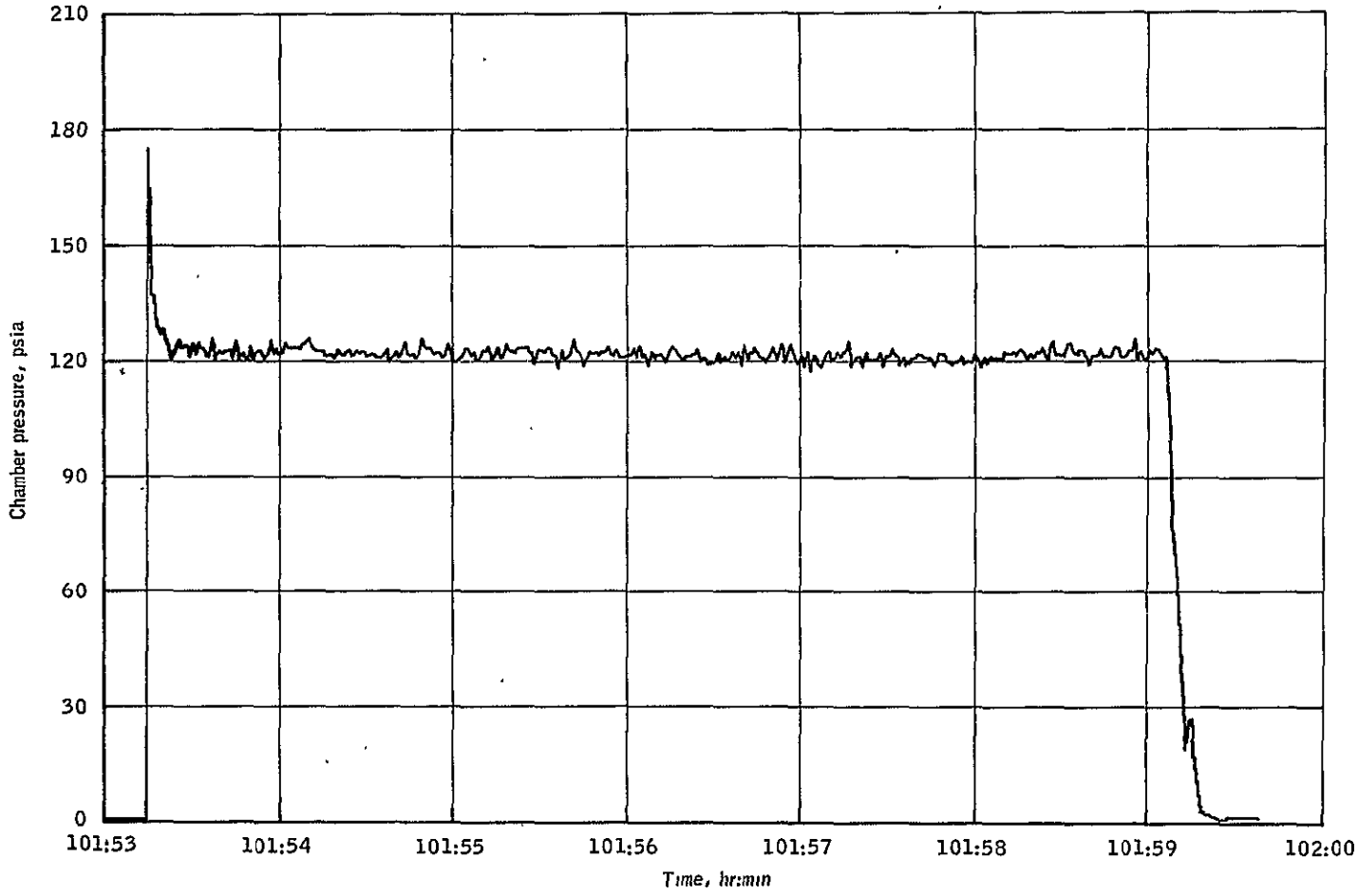

FIGURE 22- CHAMBER PRESSURE DURING APS BURN TO DEPLETION (BTD)

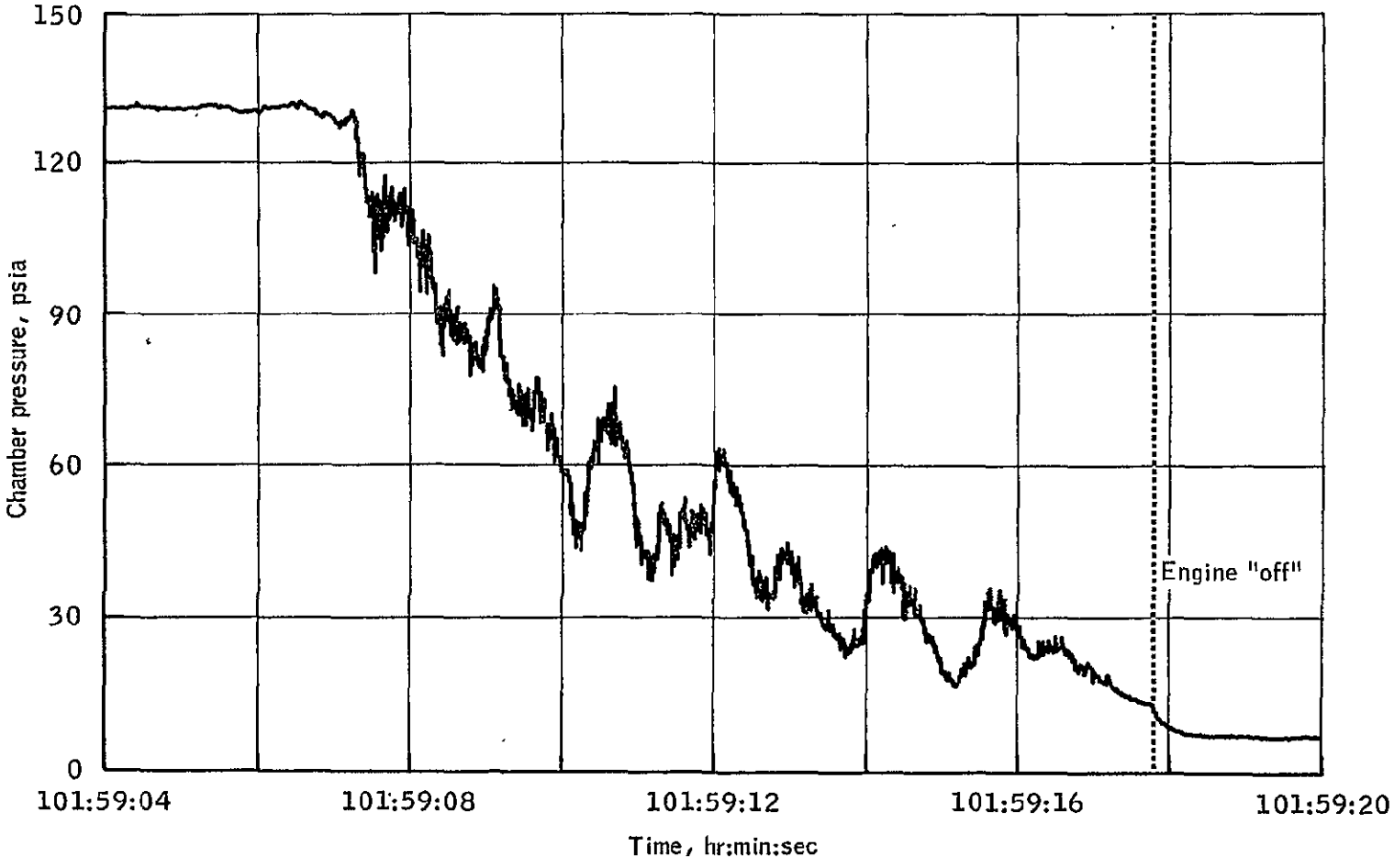

FIGURE 23.- CHAMBER PRESSURE DURING APS OXIDIZER DEPLETION

APPENDIX A

FLIGHT DATA

Figure